nature biomedical engineering

ARTICLES

https://doi.org/10.1038/s41551-020-00674-w

Check for updates

Mechanobiological conditioning of mesenchymal stem cells for enhanced vascular regeneration

Jason Lee[1], Kayla Henderson[1], Miles W. Massidda[1], Miguel Armenta-Ochoa[1], Byung Gee Im[1], Austin Veith[1], Bum-Kyu Lee[2], Mijeong Kim[2], Pablo Maceda[1], Eun Yoon[1], Lara Samarneh[1], Mitchell Wong[1], Andrew K. Dunn[1], Jonghwan Kim[2] and Aaron B. Baker[1,2,3,4]✉

Using endogenous mesenchymal stem cells for treating myocardial infarction and other cardiovascular conditions typically results in poor efficacy, in part owing to the heterogeneity of the harvested cells and of the patient responses. Here, by means of high-throughput screening of the combinatorial space of mechanical-strain level and of the presence of particular kinase inhibitors, we show that human mesenchymal stem cells can be mechanically and pharmacologically conditioned to enhance vascular regeneration in vivo. Mesenchymal stem cells conditioned to increase the activation of signalling pathways mediated by Smad2/3 (mothers against decapentaplegic homolog 2/3) and YAP (Yes-associated protein) expressed markers that are associated with pericytes and endothelial cells, displayed increased angiogenic activity in vitro, and enhanced the formation of vasculature in mice after subcutaneous implantation and after implantation in ischaemic hindlimbs. These effects were mediated by the crosstalk of endothelial-growth-factor receptors, transforming-growth-factor-beta receptor type 1 and vascular-endothelial-growth-factor receptor 2. Mechanical and pharmacological conditioning can significantly enhance the regenerative properties of mesenchymal stem cells.

Cell-based therapies could treat diseases that are not amenable to traditional treatments. Therapies based on mesenchymal stem cells (MSCs) are particularly appealing, as they are a source of autologous cells with multipotency, and can be collected from patients with relative ease. MSCs may also be able to self-renew[1,2] and have immunosuppressive properties that make them potential candidates for autologous cellular therapeutics[3]. For cardiovascular therapies, MSCs have been explored for the treatment of myocardial infarction and of peripheral ischaemia[4–9]. However, these trials have not shown consistent long-term benefits to patients[10–13]. MSCs have several aspects that limit their potential for use in cell therapies. In conventional culture conditions, MSCs lose their differentiation potential and have reduced therapeutic properties after expansion[14,15]. Furthermore, the isolated MSC populations have a high degree of heterogeneity, with subsets of cells that have varying degrees of potential for inducing regeneration[16,17]. Moreover, the therapeutic potential of MSCs is altered by the health of the patient from whom they are collected. This is a major limitation, as patients with advanced age, obesity, diabetes and other chronic disorders have MSCs with reduced regenerative properties[14,15,18–21]. Thus, those patients who would probably benefit the most from cell therapies are those who have the least-regenerative MSCs. Genetic modification of MSCs could potentially address some of these issues but would also raise concerns of tumorigenicity[22]. As a consequence, there is an intense interest in identifying alternative strategies for making MSCs more effective and reliable despite the patient-to-patient differences in MSC behaviour and reduced inherent regenerative ability.

The differentiation of MSCs into vascular cell types would be highly advantageous for many clinical applications, including the treatment of ischaemia and in tissue engineered vascular grafts. Unfortunately, there is not a consensus in the field regarding the conditions that induce endothelial differentiation in MSCs or even if the phenotype obtained is truly endothelial in nature[23–26]. Biophysical forces, including shear stress and mechanical stretch, have been used to condition MSCs into vascular phenotypes[27–32]. Several studies have shown that shear stress and treatments, such as VEGF, can lead to the expression of endothelial markers in MSCs[23,25]. However, some studies have found contrasting results in endothelial differentiation for identical treatments or an increase in markers for vascular smooth muscle cells (vSMCs) in addition to those for endothelial cells (ECs)[31–34]. It is therefore unclear what conditions are optimal for obtaining an endothelial-cell-like phenotype in MSCs. Moreover, it is unclear whether enhancing the endothelial or vascular phenotype also increases the effectiveness of MSC therapies.

In this Article, we used a high-throughput system for applying mechanical stretch to cultured cells to examine the ability of applied mechanical forces to enhance the regenerative properties of MSCs. Using this system, we performed a set of powerful screening assays that examined the synergy between biochemical factors, pharmacological inhibitors and biomechanical forces in conditioning MSCs into vascular-cell-like phenotypes that have enhanced regenerative properties. We identified specific mechanical conditions that induce maximal activation of the YAP and Smad2/3-mediated signalling pathways in MSCs. Using a high-throughput screen incorporating applied mechanical load, we also identified pharmacological inhibitors that synergistically activated these pathways. A rigorous analysis of the phenotype of the cells treated with combined mechanical conditioning and drug treatments revealed increased expression of both pericyte and endothelial markers. These optimally conditioned MSCs exhibited enhanced pericyte

[1]Department of Biomedical Engineering, University of Texas at Austin, Austin, TX, USA. [2]Institute for Cellular and Molecular Biology, University of Texas at Austin, Austin, TX, USA. [3]The Institute for Computational Engineering and Sciences, University of Texas at Austin, Austin, TX, USA. [4]Institute for Biomaterials, Drug Delivery and Regenerative Medicine, University of Texas at Austin, Austin, TX, USA. ✉e-mail: abbaker@austin.utexas.edu

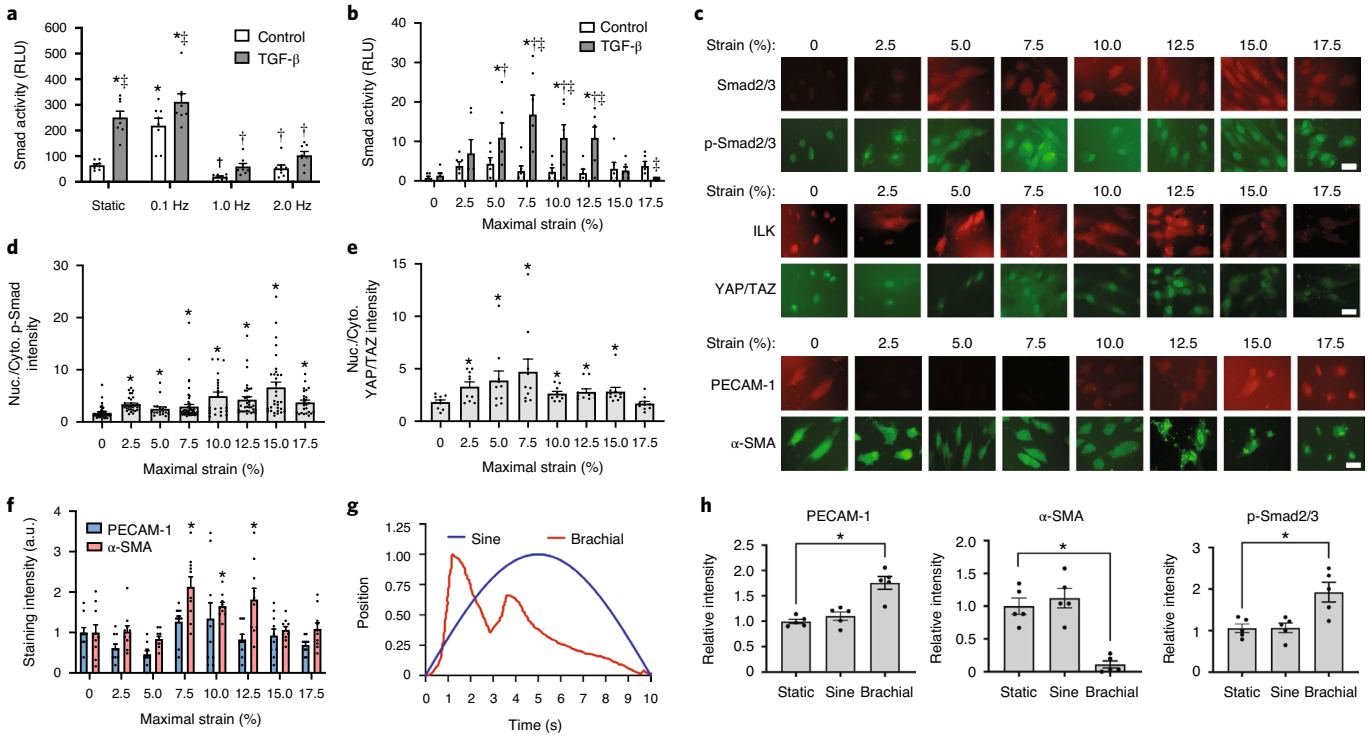

Fig. 1 | Specific types of mechanical stretch activate Smad2/3 and YAP/TAZ pathways in MSCs. a, Transcription factor activity in MSCs was measured using a luciferase reporter assay after the application of cyclic mechanical strain (5% maximal strain) for 8 h with co-treatment with 10 ng ml^{-1} VEGF-A or 10 ng ml^{-1} TGF-β1. $n=8$. *$P=0.001$ versus the static control group. †$P=0.001$ versus the static group treated with TGF-β1. ‡$P=0.024$ versus the control group under the same mechanical loading conditions. RLU, relative luminescence units. **b**, Smad transcription factor activity in MSCs with application of load for 24 h using the multistrain configuration. $n=6$. *$P=0.024$ versus the static control group. †$P=0.038$ versus the static growth-factor-treated group. ‡$P=0.049$ versus the control group under the same mechanical loading conditions. **c**, The MSCs were treated with mechanical load using the multistrain format at 0.1 Hz for 24 h and then immunostained for markers of vascular cell differentiation or signalling pathway activation. Scale bars, 100 μm. **d**, Ratio of nuclear (Nuc.) to cytoplasmic (Cyto.) p-Smad2/3 in MSCs after mechanical loading for 24 h. *$P=0.02$ versus the static group. **e**, Ratio of nuclear to cytoplasmic YAP/TAZ in the mechanically loaded MSCs. $n=4$. *$P=0.039$ versus the static group. **f**, Quantification of PECAM-1 and α-SMA staining in MSCs after 24 h of mechanical loading at 0.1 Hz. $n=4$. *$P=0.005$ versus the static group. a.u., arbitrary units. **g**, Strain waveforms for sine and brachial loading at 0.1 Hz. **h**, Quantification of western blotting for vascular markers and signal activation after 24 h of mechanical loading. $n=4$. *$P=0.01$ versus the static and sine loaded groups.

and endothelial behaviour in vitro, production of angiogenic soluble factors, and increased therapeutic potential in enhancing blood vessel growth in animal models of subcutaneous implantation and hindlimb ischaemia.

Results

Specific types of applied mechanical load activate Smad2/3 transcription factor activity and YAP nuclear localization in MSCs. Treatment with VEGF-A and TGF-β1 has been linked to the differentiation of MSCs into vascular cell types and other lineages[23,25,35]. We recently developed a system that enables the application of mechanical stretch in a high-throughput format with 576 individual culture wells with mechanical load[36–38]. Using this system, we explored whether there was synergy between biochemical and mechanical stimuli to activate the transcription factors by exposing the cells to VEGF-A or TGF-β1 during mechanical loading. We transduced MSCs with lentiviruses expressing luciferase reporter constructs for Smad2/3 and selected these to obtain a stable reporter cell line. We found that low-frequency mechanical loading (0.1 Hz, 5% maximal strain) activated *Smad2/3* transcription, whereas higher frequencies of loading did not (Fig. 1a). Furthermore, there was synergy in *Smad2/3* transcription with TGF-β1 treatment and mechanical loading at 0.1 Hz, and this was suppressed by loading at 1 Hz or 2 Hz (Fig. 1a). Using a multistrain configuration of the device, we performed a dose–response analysis for the magnitude of mechanical strain and found maximal activation of Smad2/3 in the presence of TGF-β1 and 7.5% cyclic mechanical strain (Fig. 1b). We repeated the studies under similar conditions and found that there was a maximal nuclear localization of YAP at 7.5% strain, similar to the activation of Smad2/3 (Fig. 1c–e). While we observed maximal activity of Smad2/3 in our studies at 7.5% strain, the nuclear intensity of Smad2/3 increased in loads higher than 7.5% strain, implying that there may be a repressive activity present towards Smad2/3 at higher strains. We next immunostained for markers of vascular lineage and found that there was an increase in the vSMC/myofibroblast marker α-SMA at mid-level strains (Fig. 1c,f). We costained for integrin-linked kinase, a known suppressor of the Hippo pathway[39], but did not see a significant difference with mechanical load (Fig. 1c). The loading system uses a linear motor that enables the application of complex physiological mechanical strain waveforms, including a brachial waveform that simulated the distension of the brachial artery during the cardiac cycle (Fig. 1g). We repeated loading at 0.1 Hz, 7.5% maximal strain with the sine and brachial waveforms, and then immunoblotted for vascular markers. While our primary goal was to examine the effects of a broad range of mechanical forces on MSC differentiation, the brachial loading profile is mimetic of the brachial artery and may simulate the forces that would be experienced by a MSC in or near to the artery stretching during the cardiac cycle. We found that there was an increase in the EC marker PECAM-1 and p-Smad2/3 and

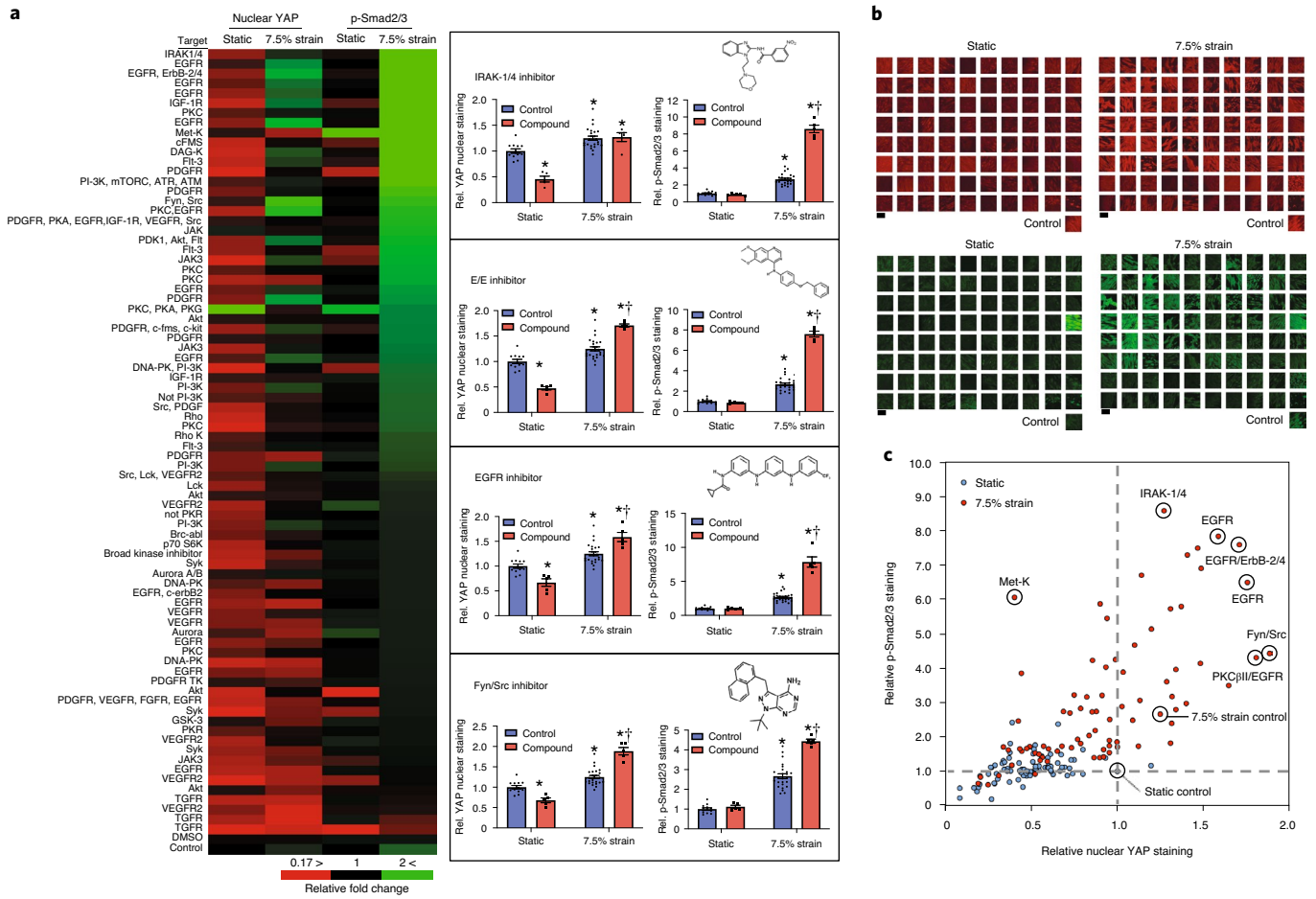

Fig. 2 | High-throughput mechanobiological screen for small-molecule inhibitors that synergistically activate YAP/TAZ and Smad2/3 with mechanical loading. MSCs were treated with 7.5% mechanical strain at 0.1 Hz for 24 h in the presence of compounds from a library of kinase inhibitors. **a**, The cells were immunostained and quantified for nuclear localization of YAP/TAZ (left) and p-Smad2/3 (right). $n = 5$. *$P = 0.037$ versus the cells treated with static conditions under the control treatment. †$P = 0.001$ versus the mechanically strained control group. Rel., relative. **b**, Images from immunostaining of cells arranged in the 96-well plate format. Upper panels show staining for YAP/TAZ (red) and lower panels show Smad2/3 staining (green). Scale bars, 50 µm. **c**, Overall summary of the mechanobiological screen separated to show the response distribution for the compounds. Labelled samples indicate the target of the inhibitor used or control treatments.

a marked decrease in α-SMA with the brachial waveform loading (Fig. 1h and Supplementary Figs. 1 and 2). To confirm that baseline and lentivirus-transduced MSCs retained their natural expression profile, we confirmed the MSC phenotype of the cells using flow cytometry (Supplementary Fig. 3). Moreover, we confirmed that the cells could differentiate into adipogenic and osteogenic lineages at the passage used (Supplementary Fig. 4).

High-throughput drug screening assay with mechanical load identifies kinase inhibitors that enhance Smad2/3 signalling and Hippo pathway activation in synergy with mechanical load. We next used the mechanical loading system to perform a screening assay to identify compounds that could enhance Smad and Hippo pathway activation in combination with mechanical load. We performed mechanical loading on MSCs in the 96-well format in the presence of one of 80 compounds from a kinase-inhibitor library. After 24 h, we immunostained for phosphorylated Smad2/3 (p-Smad2/3) and YAP/TAZ (WW domain-containing transcription regulator protein 1), and then quantified the nuclear staining of both signalling intermediates (Fig. 2a,b and Supplementary Figs. 5 and 7). From this assay, we identified compounds that substantially increased both nuclear YAP and p-Smad2/3 (Fig. 2). Many of the top hits from the assay included inhibitors of the EGFR pathways (Fig. 2c). We chose the EGFR/ErbB-2/4 (E/E) inhibitor *N*-(4-((3-chloro-4-fluorophenyl)amino)pyrido[3,4-d]pyrimidin-6-yl)2-butynamide (CAS 881001-19-0) and the PKCbII/EGFR inhibitor 4,5-bis(4-fluoroanilino)-phthalimide (CAS 145915-60-2) for further study on the basis of the maximal activation of both pathways and maximal activation of the Hippo pathway, respectively. We performed immunostaining analysis on treated MSCs from a different donor and found a weak correlation between PECAM-1/α-SMA and p-Smad2/3 (Supplementary Fig. 8a–c) and a moderately strong correlation between these markers and nuclear YAP/TAZ (Supplementary Fig. 8d–f).

Brachial waveform mechanical loading and pharmacological inhibition induce a hybrid endothelial/pericyte phenotype in MSCs with enhanced angiogenic properties. The induction of the endothelial phenotype in MSCs would be advantageous in many therapeutic applications. Unfortunately, several studies on the endothelial differentiation of MSCs have shown contradictory results[23,25,26]. Recent studies have also suggested that MSCs may be related or identical to pericytes[40]. However, other studies do not support that pericytes have stem-cell-like properties[41]. Pericyte

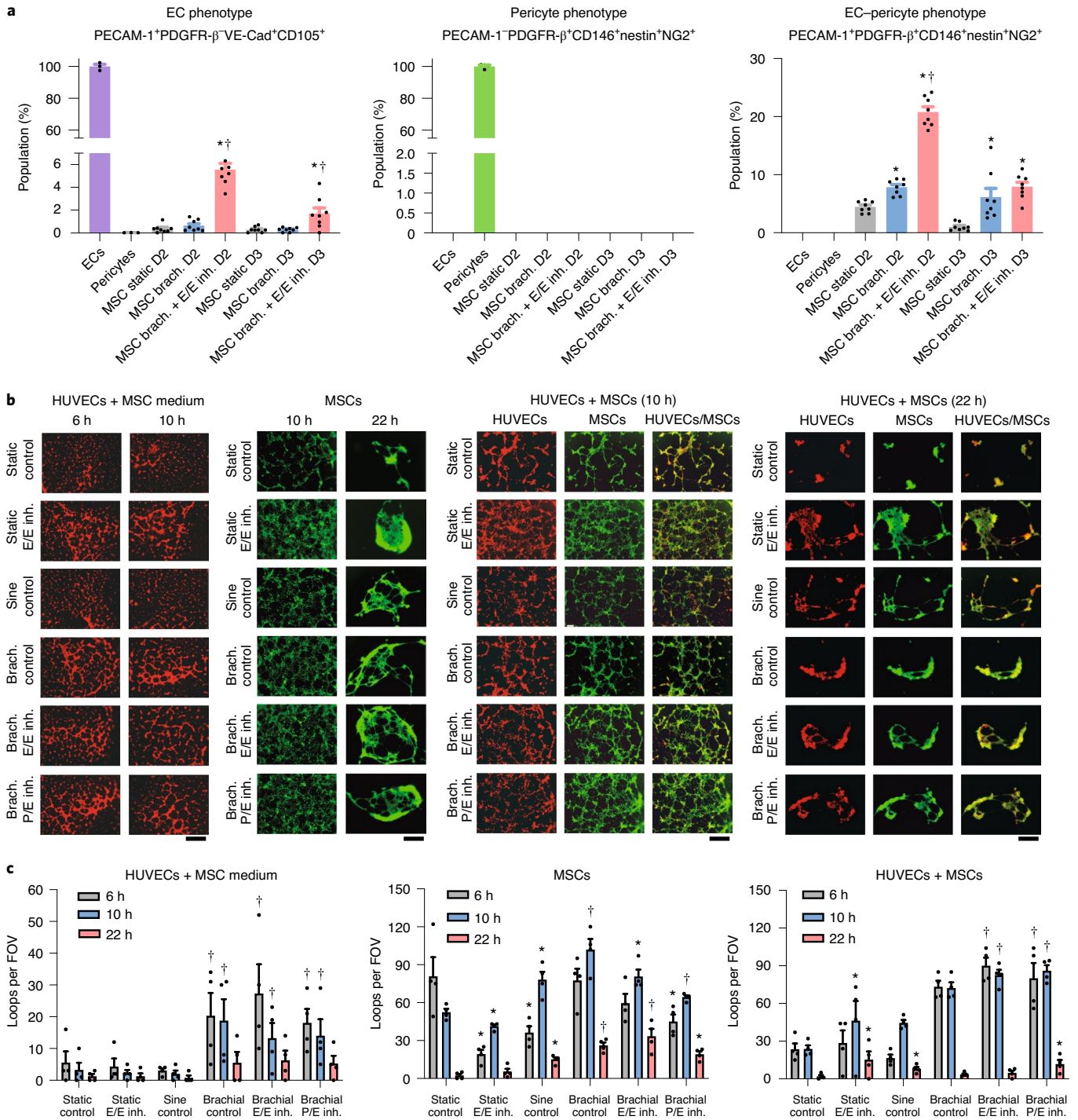

Fig. 3 | Biomechanical stimulation of MSCs with the brachial waveform and specific small-molecule inhibitors leads to increased expression of EC and pericyte markers and enhanced pericyte-like activity. a, Analysis of cells treated with biochemical factors and/or small-molecule inhibitors (inh.) for 7 d with 4 h a day of mechanical loading. Cells were labelled for multiple markers of endothelial and pericyte lineage and analysed using flow cytometry. $n = 8$ (MSCs) and $n = 3$ (ECs/pericytes). MSCs were derived from donor 2 (D2) or donor 3 (D3). *$P = 0.004$ versus the control/non-loaded group. †$P = 0.006$ versus the brachial loaded (brach.) group. **b**,**c**, Imaging (**b**) and quantification (**c**), via a tube-formation assay, of the activity of the conditioned media derived from MSCs for the indicated treatments; $n = 4$. *$P = 0.048$ versus the static group at the same time point. MSCs were derived from donor 1. †$P = 0.021$ versus the static and sine loaded groups at the same time point. Scale bars, 500 μm. FOV, field of view; P/E, PKCbII/EGFR.

markers in MSCs are correlated with enhanced regenerative properties in MSCs[42–45]. Many studies have assayed only one or two markers to define an endothelial cell or vSMC phenotype, making the true phenotype of the cells difficult to assess. To address these issues, we applied a combinatorial set of mechanical loading and biochemical/pharmacological treatments to MSCs and then assessed their phenotype by analysing multiple markers using flow cytometry (Supplementary Fig. 9). We included in the treatments the pharmacological inhibitors that were identified in the high-throughput screen that synergistically activated p-Smad2/3 and induced

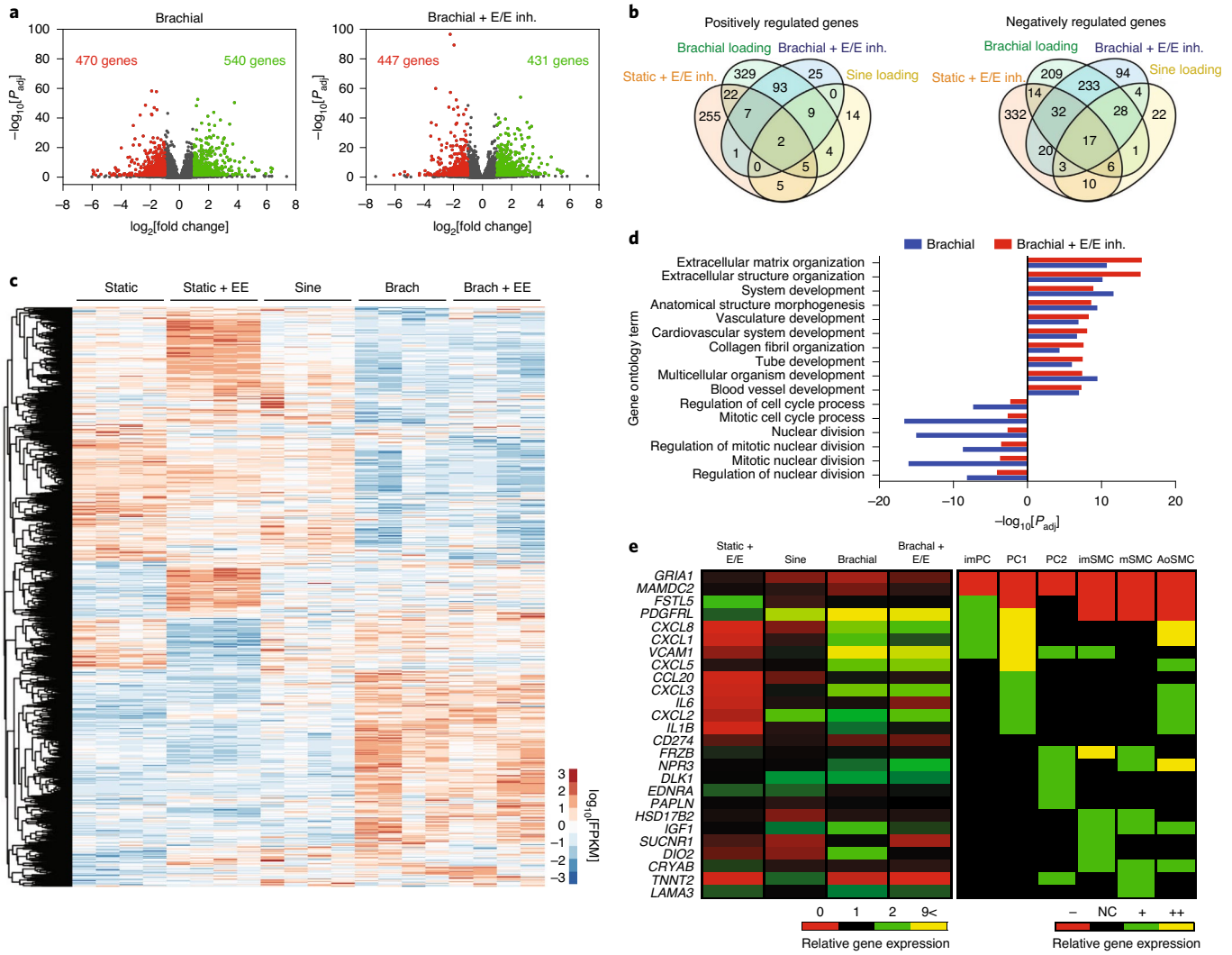

Fig. 4 | Gene expression analysis using RNA-seq demonstrates that mechanical conditioning with brachial waveform loading enhances pericyte and EC gene expression. MSCs were treated with mechanical load and/or E/E inhibitor for 7 d. **a**, Differential gene expression in comparison to the static control group. Genes with statistically significant upregulation (green) or downregulation (red) are shown in colour. **b**, Significantly upregulated and downregulated genes. **c**, Clustering analysis of the gene expression in the MSCs for significantly regulated genes. FPKM, fragments per kb of transcript per million mapped reads. **d**, Gene ontology analysis of significantly regulated gene groups. **e**, Comparison between gene expression in the treated cells and the change in gene expression in bone marrow MSCs when they differentiate into mural phenotypes[47]. The cell phenotypes listed are as follows: immature pericytes (imPC), type 1 pericytes (PC1), type-2 pericytes (PC2), immature vSMCs (imSMCs), mature vSMCs (mSMCs) and aortic vSMCs (AoSMCs). NC, no change.

YAP/TAZ nuclear localization, as well as treatments from previous studies that led to vascular cell differentiation. Using a rigorous definition for EC phenotype that required expression of multiple endothelial markers, there was little endothelial lineage expressed by the cells under baseline conditions and with the treatments. Notably, VEGF did not increase the EC lineage in the MSCs, as defined by multiple markers using flow cytometry (Supplementary Fig. 10). Furthermore, there was only a very small proportion of cells expressing all of the marker profile of pericytes (PECAM-1$^-$CD105$^-$VE-Cad$^-$CD146$^+$nestin$^+$PDGFR-β$^+$ cells). With brachial waveform mechanical loading, there was an increase in cells with both endothelial markers (PECAM-1, VE-Cad and CD105) and markers for pericytes (CD146, nestin and PDGFR-β). This population was also largely positive for NG2, suggesting a hybrid phenotype of type-2 pericytes and ECs (Supplementary Fig. 10). This EC–pericyte population was markedly increased after treatment with brachial loading and co-treatment with kinase inhibitors identified from drug screening assay to activate p-Smad2/3 and YAP (Supplementary Fig. 10). To test the robustness of these findings, we repeated some of the treatments in two additional donors and analysed their marker expression using flow cytometry in mature cell lines (ECs and pericytes) as standards for each phenotype (Supplementary Fig. 11). This analysis demonstrated an increase in the subpopulation with markers for ECs and pericytes for MSCs treated with brachial loading and the E/E inhibitor for both donors (Fig. 3a). Furthermore, there was an increase in cells with the EC phenotype in MSCs treated with brachial waveform loading + E/E inhibitor (Fig. 3a), although this population was much smaller than the EC–pericyte population. At the baseline, the MSCs had a mid-range expression of PECAM-1 compared with pericytes and ECs. To assess whether the MSCs expressed markers at similar levels to the mature cell lines, we compared the staining intensities within the gated populations (Supplementary Fig. 12). The level of expression of PECAM-1, CD144 and CD105 in the EC–pericyte population in the MSCs treated with brachial waveform loading and the E/E inhibitor was similar to that of mature ECs. Moreover,

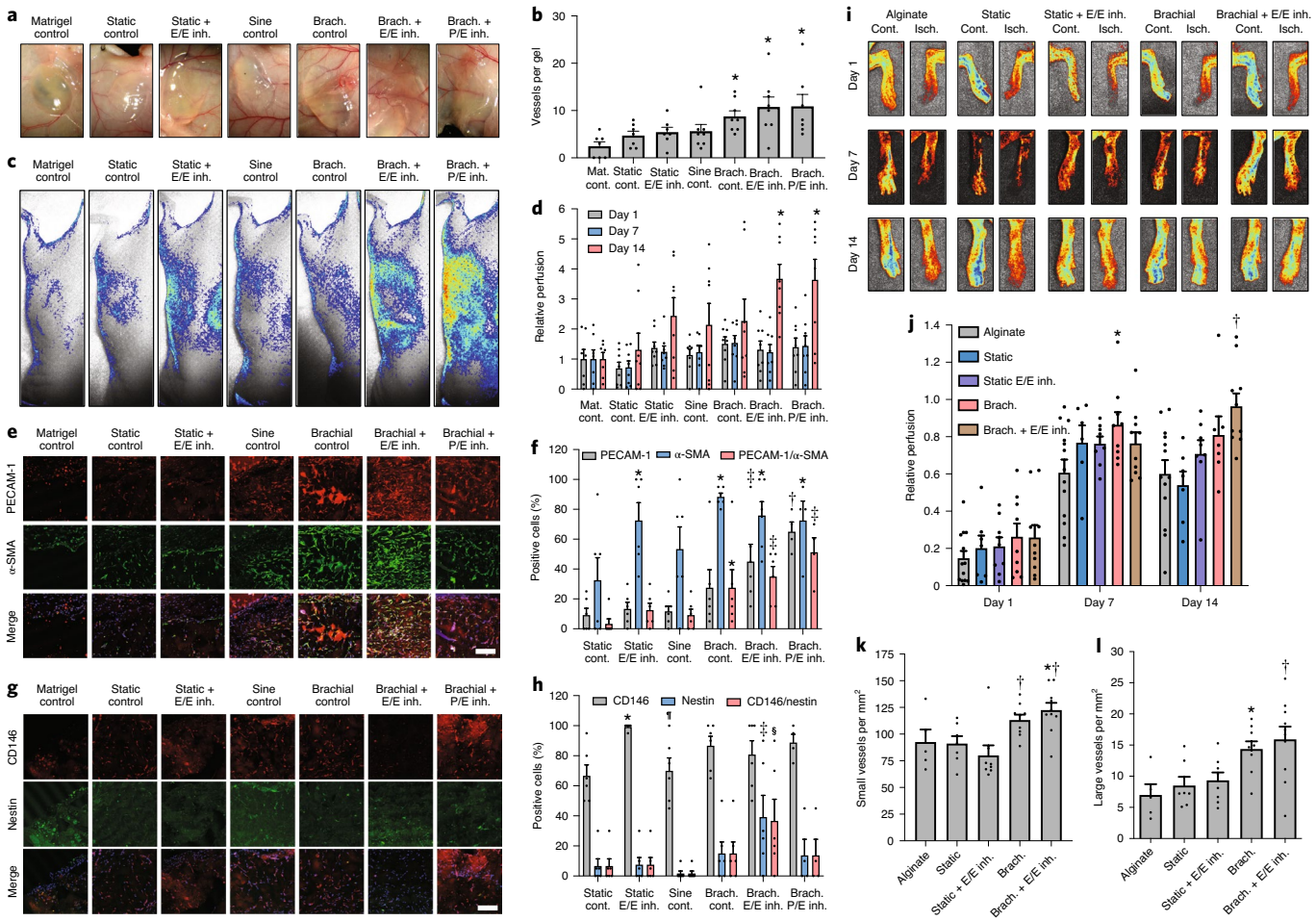

Fig. 5 | Optimized mechanical and pharmacological conditioning of MSCs increases their ability to induce angiogenesis and arteriogenesis after subcutaneous implantation or in a hindlimb ischaemia model. MSCs were treated under the indicated conditions for 7 d in culture and then implanted subcutaneously in nu/nu mice in Matrigel. **a**, Photographs of the implants after 14 d of implantation. **b**, Quantification of blood vessels in the gel using macroscopic images of the gel. *P = 0.049 versus the Matrigel (Mat.), static, static + E/E inhibitor and sine loaded groups. n = 6. cont., control. **c**, Laser speckle imaging of the mice after 14 d of implantation. **d**, Quantification of perfusion measured using laser speckle imaging after implantation. n = 6. *P = 0.049 versus the Matrigel and static control groups. **e**, Images of tissue sections from the gel regions of the explanted tissues immunostained for PECAM-1 and α-SMA. Scale bar, 100 μm. **f**, Quantification of the percentage of cells that are positive for the indicated markers. n = 6. *P = 0.049 versus static control groups. †P = 0.017 versus the static, static with E/E inhibitor, sine loaded and brachial loaded groups. ‡P = 0.021 versus the static, static + E/E inhibitor and sine loaded groups. **g**, Images of tissue sections immunostained for CD146 and nestin. Scale bar, 100 μm. **h**, Quantification of the percentage of cells that are positive for the indicated markers. *P = 0.049 versus the static control group. n = 6. †P = 0.049 versus the static, static + E/E inhibitor, sine loaded and brachial loaded groups. ‡P = 0.049 versus static, static + E/E inhibitor and sine loaded groups. §P = 0.044 versus static and sine loaded groups. ¶P = 0.004 versus the static + E/E inhibitor group. **i**, Laser speckle imaging of the feet of mice implanted with MSCs treated for 7 d with the indicated treatments. Isch., ischaemic. **j**, Quantification of the perfusion in the feet of the mice after induction of hindlimb ischaemia. n = 7 (static and brachial loading groups), n = 8 (static + EE group), n = 10 (brachial loading + EE group) and n = 13 (alginate control group). *P = 0.049 versus the alginate group. †P = 0.007 versus the alginate and static groups. **k**, Quantification of the number of small blood vessels in the thigh muscle of the ischaemic limb in the mice implanted with MSCs conditioned with the treatments. n = 5 (alginate control group), n = 7 (static group), n = 8 (static + EE and brachial loading groups) and n = 10 (brachial loading + EE groups). *P = 0.042 versus the static group. †P = 0.026 versus the static + EE group. **l**, Quantification of large vessels in the thigh muscle of the ischaemic limb of the mice. n = 5 (alginate control group), n = 7 (static group), n = 8 (static + EE and brachial loaded groups) and n = 10 (brachial loading + EE group). *P = 0.049 versus the alginate group. †P = 0.035 versus the alginate, static and brachial loading + EE groups.

the EC–pericyte population from MSCs that were treated with brachial waveform loading and E/E inhibitor had similar expression of PDGFR-β, lower expression of CD146 and NG2, and higher expression of nestin compared with pericytes. We also analysed the cells using a live–dead assay to exclude the possibility that this population was composed of dead cells (Supplementary Fig. 13). To investigate whether this population exists in the bone marrow in vivo, we sorted fresh bone marrow mononuclear cells and found that a small population that expressed both PECAM-1 and PDGFR-β markers (~0.046% of bone marrow mononuclear cells; Supplementary Fig. 14). However, we did not observe a population that expressed the full set of EC/pericyte markers. We did not observe cells with the full set of EC/pericyte markers. These findings suggest that there may be a related phenotype in the bone marrow, but the full phenotype is not present or is very rare.

Biomechanical conditioning increases the pericyte-like activity and angiogenic properties of MSCs. We next examined whether the cells under the different conditions had increased pericyte-like behaviour and proangiogenic activity using a tube formation assay.

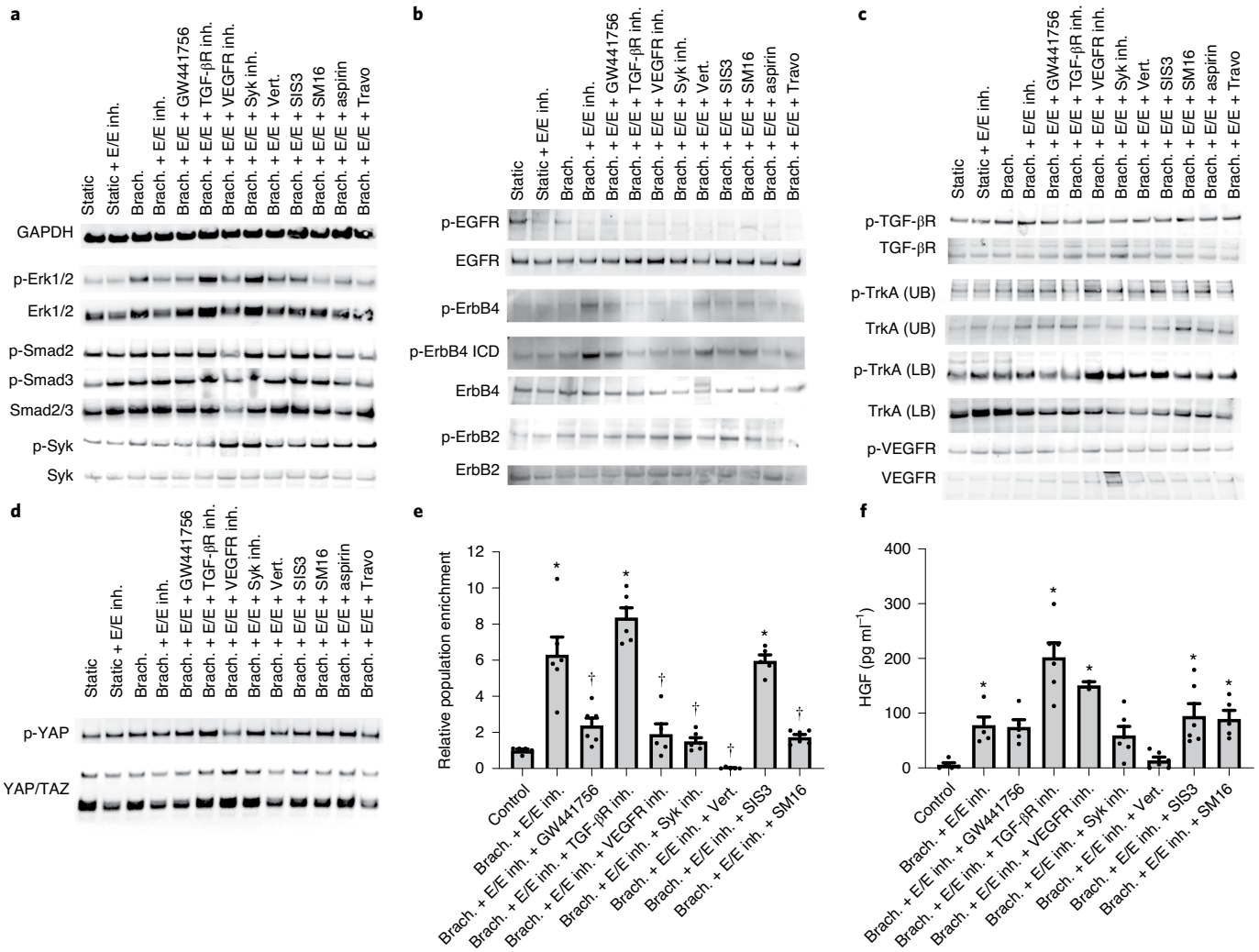

Fig. 6 | Analysis of cell signalling pathways activated during treatment of MSCs with brachial waveform loading with an E/E inhibitor. a, Western blotting analysis of cells for GAPDH and signalling through the Erk1/2, Smad2/3 and Syk pathways after treatment with mechanical loading and E/E inhibitor with the addition of inhibitors as indicated. The inhibitors included a TrkA inhibitor (GW441756), TGF-βR1 inhibitor (TGF-βR inh.), VEGFR2 inhibitor (VEGFR inh.), Syk inhibitor (Syk inh.), YAP inhibitor verteporfin (Vert.), Smad3 inhibitor (SIS3), Smad2 inhibitor (SM16), aspirin and prostaglandin F2α agonist travoprost (Travo). **b**, Western blotting analysis of cells for signalling through the EGFR, ErbB2 and ErbB4 pathways after treatment with mechanical loading and E/E inhibitor with the addition of inhibitors as indicated. **c**, Western blotting analysis of cells for signalling through the TGF-βR, TrkA and VEGFR2 pathways after treatment with mechanical loading and E/E inhibitor with the addition of inhibitors as indicated. **d**, Western blotting analysis of cells for signalling through the YAP/TAZ pathways after treatment with mechanical loading and E/E inhibitor with the addition of inhibitors as indicated. **e**, Flow cytometry analysis of cells for EC/pericyte phenotype after treatment with mechanical load and inhibitors as indicated for 7 d. The EC/pericyte phenotype was defined as having the following marker expression: $PECAM\text{-}1^{+}PDGFR\text{-}\beta^{+}VE\text{-}CAD^{+}CD105^{+}CD146^{+}nestin^{+}NG2^{+}$. $n=6$. $^{*}P=0.001$ versus the static control group. $^{\dagger}P=0.001$ versus the brachial loading + EE group. **f**, ELISA analysis of the production of HGF in conditioned medium from MSCs treated as indicated for 7 d. $n=8$. $^{*}P=0.04$ versus the control group.

Conditioned media from MSCs treated with brachial loading with or without pharmacological inhibitors induced increased tube formation in ECs (Fig. 3b and Supplementary Fig. 15a). We also plated the MSCs on Matrigel directly and found that there was increase in the formation of mature tubes at later time points (Fig. 3b and Supplementary Fig. 15b). We next mixed MSCs with ECs and plated them together to examine the effect of mechanical/biochemical conditioning on inducing pericyte-like behaviour in MSCs. This analysis showed that MSCs that were exposed to brachial waveform loading had increased tube formation in co-culture with ECs (Fig. 3b and Supplementary Fig. 15c). We performed mechanical loading of MSCs with the sine and brachial waveforms (4 h per day) and treated the cells with pharmacological inhibitors for 7 d (the compounds were not added in the final day treatment). The conditioned media from MSCs under the treatments were found to decrease EC proliferation compared with the conditioned medium from cells that were grown under control conditions (Supplementary Fig. 16).

Next, we examined the production of growth factors by MSCs under mechanical loading with co-treatment of pharmacological inhibitors after short-term (24 h) or longer-term (7 d) treatment. We performed an antibody array analysis of the conditioned medium from the treated cells and identified alterations in growth factor production by the MSCs after 24 h or 7 d of loading with the

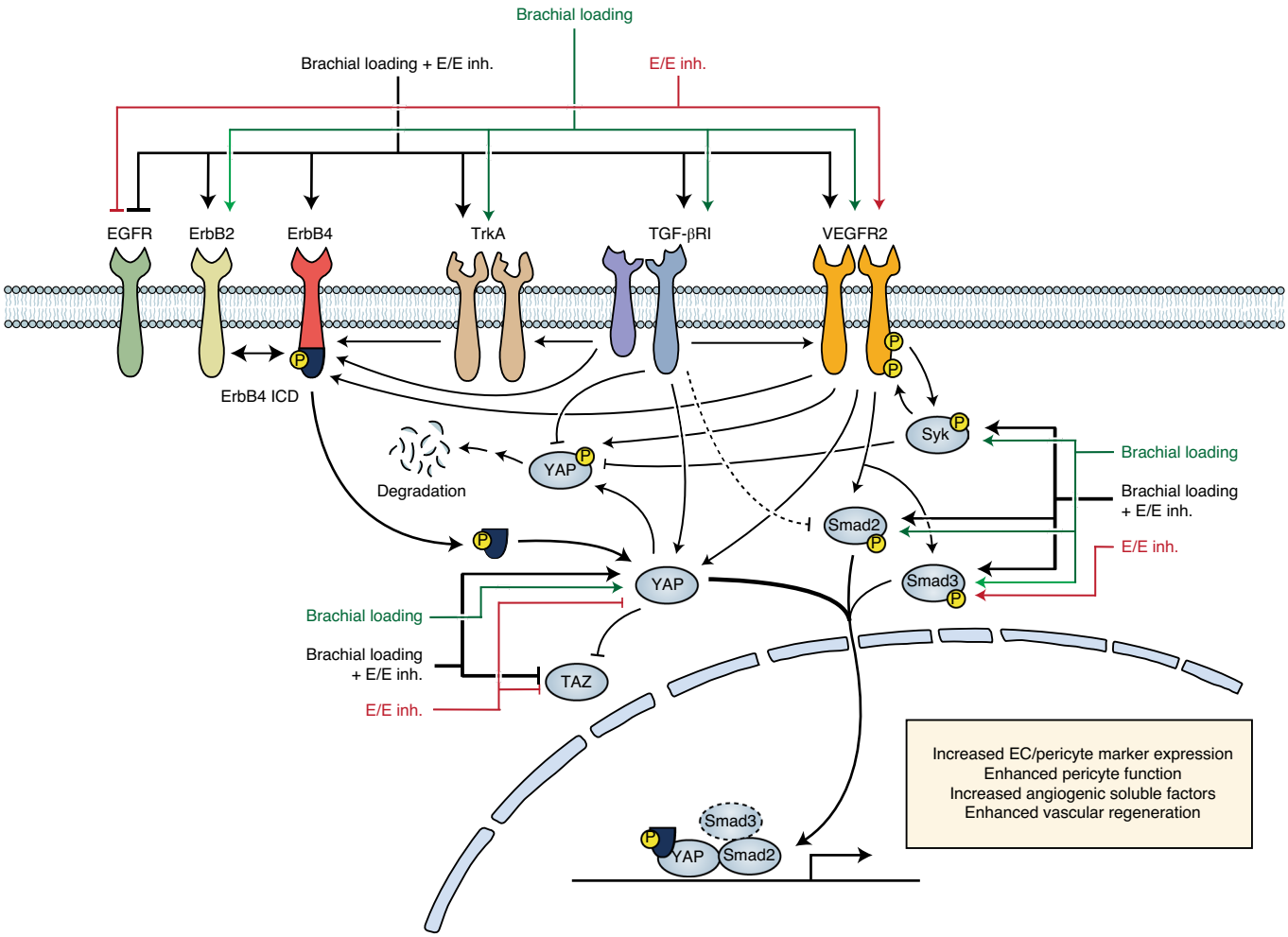

Fig. 7 | Summary of mechanism for mechanical conditioning of MSCs. Diagram of the hypothesized mechanism for regulating the development of ECs/pericytes in MSCs by mechanical loading and E/E inhibition.

co-treatments (Supplementary Fig. 17). We used enzyme-linked immunosorbent assays (ELISA) to measure changes in the growth factors and found increases in angiotensin-1 (Ang-1) and VEGF-A with sine-wave loading after 24 h (Supplementary Fig. 18). After 7 d of loading, there was a marked increase in hepatocyte growth factor (HGF)—a proangiogenic growth factor[46]—in all of the groups treated with mechanical load (Supplementary Fig. 19). In the groups treated with brachial loading, there was also a decrease in TGF-β1, Ang-1 and Ang-2 (Supplementary Fig. 19). From the antibody array assay, although there were increases angiogenic factors in the groups treated with the sine and brachial waveforms, there was a marked decrease in the antiangiogenic factors angiostatin and prolactin in only the brachial loading + E/E group. Thus, the tube formation response may reflect both a gain of proangiogenic factors and a loss of antiangiogenic factors in the brachial E/E group.

We performed a proliferation assay after treatments of the cells and found that brachial waveform mechanical loading leads to increased proliferation of the MSCs after passaging the cells in polystyrene culture dishes (Supplementary Fig. 20). To examine whether the treatments led to adipogenic or osteogenic differentiation, we stained the cells with Oil Red O or Alizarin Red S but did not find significant changes in the staining in comparison to the static conditions (Supplementary Fig. 21). We also performed immunostaining for early markers of osteogenic and adipogenic differentiation, but did not observe significant changes in these with the treatments (Supplementary Fig. 22). Furthermore, we grew the cells to confluency and immunostained for VE-cadherin but did not find cell–cell junctions with VE-cadherin enrichment (Supplementary Fig. 23). However, we did observe an overall increase in VE-cadherin in the brachial loading + E/E inhibitor group. There was no difference between the cells in terms of barrier function, as measured using a permeability assay (Supplementary Fig. 24) and measurements of transepithelial electrical resistance (Supplementary Fig. 25).

Gene expression analysis using RNA-seq demonstrates enhancement of pericyte/endothelial phenotypes and proangiogenic gene expression in MSCs with optimized mechanical conditioning and small-molecule inhibitor treatment. To further examine whether mechanical loading and drug treatment enhanced the angiogenic and pericyte-like phenotype in MSCs, we performed RNA-sequencing (RNA-seq) analysis of MSCs under the various treatments. A differential gene expression analysis revealed that treatment with the brachial waveform mechanical loading, with or without the E/E inhibitor, significantly regulated a large number of genes in comparison to the sine waveform (Fig. 4a,b). Treatment with the E/E inhibitor also modulated a relatively large number of genes (Supplementary Fig. 26). Cells treated with either brachial loading or brachial loading + E/E inhibitor showed similar patterns of gene expression, whereas MSCs treated with sine loading or static conditions were more similar (Fig. 4c). Gene Ontology analysis of

the changes in the gene expression revealed significant increases in gene expression for ECM remodelling, vasculature development and tube formation after treatment with brachial waveform loading and brachial loading + E/E inhibitor (Fig. 4d). To examine the development of the pericyte-like phenotype, we compared the gene expression of the cells in our study to the results of a gene expression analysis from another study that examined the development of pericytes and vSMCs from mesenchymal cells[47]. For cells treated with brachial loading and brachial loading + E/E, there were changes in gene expression consistent with a pericyte phenotype (Fig. 4e). We examined a set of genes that is associated with the development of the endothelial phenotype[48] and found that some, but not all, of these genes were strongly upregulated (Supplementary Fig. 27). We also examined the gene expression for soluble factors related to angiogenesis, and we found increases in ANGPT2 and HGF for the cells treated with static + E/E inhibitor, brachial loading and brachial loading + E/E inhibitor (Supplementary Fig. 28). To further investigate whether the brachial loading with E/E inhibitor treatment promotes differentiation of MSCs into ECs or pericytes, we next performed gene set enrichment analysis (GSEA) on the RNA-seq datasets[49]. We found a strong enrichment of both EC and pericyte gene sets in the MSCs treated with mechanical load and mechanical load + E/E inhibitor compared with the control cells (Supplementary Fig. 29).

Optimized mechanical and pharmacological conditioning of MSCs increases proangiogenic potential in vivo. We next examined the effects of mechanical loading and pharmacological conditioning on the in vivo angiogenic properties of MSCs. We conditioned the cells with the treatments for 7 d and then implanted them subcutaneously into nu/nu mice. After 14 d, there were increased numbers of vessels invading the gels implanted with MSCs exposed to brachial waveform mechanical loading on the basis of the macroscopic images of the implant (Fig. 5a,b). In particular, the cells treated with the brachial waveform loading and pharmacological co-treatment had the highest number of large vessels invading. Analysis using laser speckle imaging revealed increased perfusion in the skin over the implants of the groups treated with the brachial-waveform-loaded MSCs with pharmacological co-treatment, consistent with the macroscopic appearance of the implants (Fig. 5c,d). Histological analysis of the gels also demonstrated increased PECAM-1$^+$ and α-SMA$^+$ cells, as well as PECAM-1$^+$α-SMA$^+$ double-positive cells, in samples treated with brachial waveform loading in combination with pharmacological inhibitor (Fig. 5e,f). Furthermore, there was an increase in nestin$^+$ cells, as well as nestin$^+$CD146$^+$ double-positive cells, in samples treated with brachial loading + E/E inhibitor (Fig. 5g,h). There were also marked increases in platelet-derived growth factor receptor beta (PRGFRβ$^+$) and PECAM-1$^+$PDGFR-β$^+$ cells in samples treated with brachial loading + E/E inhibitor (Supplementary Fig. 30a,b). We assessed proliferating cells in the Matrigel using staining for Ki-67 and found that only the static cells with co-treatment of E/E inhibitor had increased numbers of proliferating cells (Supplementary Fig. 30c,d). To confirm that the cells in the Matrigel were primarily derived from the MSCs that were delivered, we performed fluorescence in situ hybridization (FISH) for the human X chromosome (Supplementary Fig. 31). Together, these findings support the concept that combined conditioning with pharmacological inhibitors and specific mechanical conditions can increase the proangiogenic properties of MSCs.

To further confirm the functional activity of the conditioned MSCs, we exposed the cells to the treatments for 7 d, encapsulated them in alginate-RGD/collagen gel and implanted them in nu/nu mice that underwent surgery to create unilateral hindlimb ischaemia through femoral artery ligation. We observed enhanced recovery of perfusion in the mice treated with cells that had been conditioned with brachial waveform loading and E/E inhibitor (Fig. 5i,j). Histological analysis revealed a moderate increase in capillaries and increases in larger mature vessels of more than twofold in the muscle from mice treated with MSCs conditioned with brachial loading or brachial loading + E/E inhibitor (Fig. 5k,l and Supplementary Fig. 32). We confirmed the continued presence of MSCs in the hindlimb of the mice using FISH for the human X chromosome (Supplementary Fig. 33). To examine whether brachial loading and E/E treatment could work for MSCs derived from other donors, we repeated the mouse hindlimb ischaemia studies using MSCs from another donor (donor 2) and measured perfusion in the legs for 28 d after induction of ischaemia. We observed enhanced recovery from ischaemia in mice treated with MSCs conditioned with brachial loading + E/E inhibitor from donor 2 as well (Supplementary Fig. 34).

Brachial waveform loading and E/E inhibition leads to EC/pericyte marker expression through a YAP- and Smad2-mediated pathway. From the kinase screen with mechanical load, we identified those pathways for which multiple inhibitors block the activation of p-Smad2/3 and YAP. Furthermore, there were many genes related to prostaglandin production/signalling were that upregulated in the RNA-seq analysis for both brachial loading and brachial loading + E/E inhibition treatment. These inhibitors included inhibitors of TrkA, TGF-βR, VEGFR2, Syk, Smad2, Smad3, YAP and COX-1/2. We treated the cells with brachial loading + E/E inhibition and inhibitors of these pathways, and then measured the signalling in the pathways using western blotting (Fig. 6a–d and Supplementary Figs. 35–38). Furthermore, we repeated these treatments and measured the expression of markers for ECs and pericytes using flow cytometry, and measured the production of HGF in the conditioned medium of the cells using ELISA (Fig. 6e,f). Combining these results with those from the kinase screen, we created a hypothesized mechanistic model of the regulation of the development of ECs/pericytes through mechanical load and E/E inhibition (Fig. 7). The upregulation of HGF production was primarily controlled through a YAP-mediated pathway (Fig. 6f).

Discussion

MSCs are an appealing cell type for use in therapies for ischaemia, but clinical trials have not yielded consistent benefits for patients. The application of MSCs in vascular regeneration and tissue engineering has been limited by contradictory or inconsistent findings in studies describing MSC differentiation into vascular phenotypes[23,26]. Using a mechanobiological screen, our studies identified conditions that enhanced MSC therapeutic activity and induced increased differentiation toward a novel phenotype with combined markers of pericytes and ECs. The increased pericyte/EC-like behaviour in the MSCs was supported by multiple orthogonal techniques, including multimarker flow cytometry, in vitro functional assays, gene expression analysis using RNA-seq and animal models. There have been several studies that support that perivascular cells may behave as MSCs in the body[40]. However, other studies suggest that pericytes are not stem cells[41]. Our study demonstrates that a hybrid pericyte–endothelial phenotype can exist in cultured MSCs and that it can be increased through combined mechanical loading and E/E inhibition.

In our mechanobiological screening assays, we found conditions that increased signalling through the p-Smad2/3 and YAP/TAZ pathways. These pathways have been linked in many previous studies to MSC differentiation into other MSC phenotypes[50]. However, the pathways are also important in angiogenesis and pericyte function. Signalling through YAP/TAZ is enhanced in the tip cells of capillaries during angiogenesis and vascular development[51–53]. Furthermore, pericyte-specific knockout of YAP and TAZ disrupts their coordination of alveologenesis by reducing their production

of HGF[54], a soluble factor that was highly upregulated by the treatments used in our studies. Signalling through Smad2/3 is required for vascular stability[55], modulates pericyte/endothelial interactions[56] and TGF-β signalling enhances the association of pericytes/mesenchymal cells to ECs[57]. There is also evidence that links Smad2/3 to endothelial differentiation in MSCs and induced pluripotent stem cells[58,59]. Moreover, YAP is localized to the nucleus in sprouting vessels and deletion of YAP and TAZ causes dramatic defects in blood vessel development[53,60]. The TGF-β pathway is key in regulating pericyte differentiation in some cell lines, regulates pericyte behaviour and is important in pericyte–EC interactions[61–64]. Here, the compounds from our high-throughput screen that activated these pathways enhanced the pericyte and EC-like phenotype of the MSCs without significant increases in osteogenic or adipogenic differentiation. Furthermore, these treatments enhanced the expression of HGF and the angiogenic potential of the soluble factors produced by the MSCs. Our studies suggest that YAP and Smad2 signalling have a complex role in regulating MSC phenotype and regenerative properties. While our screening assays focused on activation of these pathways, future screens could target enhancement of the ECs/pericytes directly and potentially achieve higher levels of enhancement of this phenotype.

Previous studies have identified that mechanical forces can increase the vascular cell phenotype of MSCs. Notably, the application of mechanical strain to MSCs increases the expression of vSMC markers[65,66] and the application of shear stress has, in some studies, been linked to the expression of EC markers[67]. There have also been mixed results in studies aiming to induce endothelial differentiation in MSCs, with some studies finding differentiation into endothelial phenotype with VEGF-A treatment while others do not show these effects[23,26,68]. Our findings using flow cytometry analysis of multiple markers suggest that there is very little pure EC differentiation of MSCs under a broad range of treatments. Given our findings of a pericyte–endothelial hybrid phenotype, even the presence of multiple endothelial markers does not exclude the possibility that the MSCs also express mural markers. Even under the most optimal conditions, only about 8% of the total MSC population expressed endothelial markers in the absence of pericyte markers. Thus, our studies suggest that previous findings of endothelial differentiation in MSCs should be viewed with the perspective that further studies may be needed to rule out hybrid phenotypes.

In summary, our findings have identified that MSCs can be conditioned into an enhanced phenotype with increased expression of markers of pericytes and ECs. The conditioning required the use of complex mechanical strain waveforms and drug treatment. We were not able to achieve improved regenerative properties from the MSCs in the absence of applied mechanical forces. Given the wide variation in MSC behaviour and loss of activity due to disease and aging, a potential approach may be to first isolate MSCs from the patient and optimize the desired phenotype using a mechanobiological screen similar to the one used in this study. For vascular regeneration, we envision that MSCs could be collected from patients and tested in a mechanobiological screen to maximize the mixed EC–pericyte population. These mechanical and biochemical/pharmacologically optimized and conditioned cells can then be implanted or injected into the patient for treatment. Thus, while the pathways and mechanical conditions that were found to be optimal in this study may be generalizable to many MSC lines, the overall optimization process of using mechanobiological screening provides a paradigm for enhancing stem cell therapies in a patient specific manner.

Methods

Construction of a high-throughput biaxial oscillatory strain system. Mechanical strain was applied to cell cultures using a high-throughput system that was described previously[36–38]. In brief, cells were cultured on custom-made plates that are mounted onto a system that applies strain. The cell culture plates comprised silicone membranes (127 µm thickness; Specialty Manufacturing) that are sandwiched between two plates, with silicone rubber gaskets at the interfaces to prevent leaking. These cell culture membranes were UV sterilized and coated with 50 µg ml^{-1} fibronectin overnight at 37 °C to allow cell adhesion. After cell attachment, the plates were mounted onto the top plate of the system using screws. To apply mechanical strain, a platen with 576 Teflon pistons was moved into the cell culture membrane. The motion is driven by a hygienically sealed, voice-coil-type linear motor (Copley Controls). The platen was stabilized using six motion rails mounted with linear motion bearings. The hygienically sealed motor housing has chilled water running through to prevent over heating during operation. The 576 pistons that come in contact with the cell culture surface can be individually adjusted to have different height, enabling precise calibration of the strain applied to each well.

Cell lines and cell culture. Human MSCs (Millipore) were cultured in low-glucose DMEM medium supplemented with 15% fetal bovine serum, L-glutamine and penicillin–streptomycin. After trypsinization, cells were seeded on the membranes at 20,000 cells per cm^2 before mechanical loading. The cells were used between passages 3–6. The MSCs were derived from a donor 1 (Asian, male, aged 22 years), unless otherwise specified. A subset of the studies was performed using MSCs from donor 2 (white, male, aged 24 years) or donor 3 (white, female, aged 32 years). Fresh bone marrow cells were obtained from a different donor from these cell lines (white, male, aged 28 years). HUVECs (PromoCell GmbH) were cultured in MCDB 131 medium supplemented with 7.5% fetal bovine serum, L-glutamine and penicillin–streptomycin and EGM-2 SingleQuot Kit (Thermo Fisher Scientific). Human brain vascular pericytes (HBVPs) were cultured in high-glucose DMEM F12 medium supplemented with 10% fetal bovine serum, L-glutamine and penicillin–streptomycin. Human aortic vSMCs were cultured in MCDB 131 medium supplemented with 10% fetal bovine serum, L-glutamine and penicillin–streptomycin. All cells were cultured in an incubator at 37 °C under a 5% CO_2 atmosphere.

Measurement of transcription factor activity. Human MSCs (passage 3) were transduced with lentiviruses for the expression of luciferase reporter constructs (Qiagen) for the target transcription factors. In brief, cells were cultured with the lentivirus (1×10^7 TU) in medium containing polybrene for 24 h. After virus incubation, the medium was replaced with normal medium for 1 d. Transduced cells were then selected with medium containing puromycin (1 µg ml^{-1}) for 3 d. After the treatments, the cells were lysed and the relative luminescent signal was measured using the luciferase assay kit (Promega) and read using the FlexStation-3 plate reader (Molecular Devices). For the measurement, each well was read three times, and the average was taken for a single data point (technical replicates). These technical replicates were averaged for biological replicates from separate wells in the data presented.

Immunocytochemical staining on silicone membranes. After the treatments, the cells were fixed in 4% paraformaldehyde in PBS for 10 min followed by washing and permeabilization with 0.1% Triton X-100 PBS for 5 min. Next, samples were blocked with PBS containing 5% fetal bovine serum (FBS) and 1% bovine serum albumin (BSA) for 40 min. After washing, cells were incubated with primary antibodies (a list of specific antibodies and concentrations is provided in Supplementary Table 1) in PBS with 1% BSA overnight at 4 °C. The samples were then washed twice in PBS with 1% BSA and incubated with secondary antibodies in PBS with 1% BSA for 2 h in a light-protected environment. Cells were washed extensively with PBS with 1% BSA before mounting in anti-fade medium (Vector Laboratories). The samples were then imaged using epifluorescence microscopy (Axio Observer; Carl Zeiss), or confocal microscopy using either an LSM 710 laser scanning confocal microscope (Carl Zeiss) or an FV10i Confocal Laser Scanning Microscope (Olympus).

Immunocytochemical staining on removable well plates. Glass-bottom plates with removable culture chambers (Ibidi) were coated with 8 µg ml^{-1} fibronectin in PBS for 4 h at 37 °C. After the mechanical and chemical treatments, the cells were seeded onto the plates at a density of 50,000 cells per well and allowed to grow for 2 d in culture medium. The cells were next washed with PBS and fixed in 4% paraformaldehyde in PBS for 10 min followed by washing and permeabilization with 0.1% Triton X-100 PBS for 5 min. Samples were then blocked with PBS containing 5% FBS and 1% BSA for 40 min. After washing, cells were incubated with primary antibodies (a list of specific antibodies and concentrations is provided in Supplementary Table 1) in PBS with 1% BSA overnight at 4 °C. The samples were then washed twice in PBS with 1% BSA and incubated with secondary antibodies in PBS with 1% BSA for 2 h in a light-protected environment. Cells were washed extensively with PBS with 1% BSA before mounting in anti-fade medium (Vector Laboratories). The samples were then imaged using confocal microscopy using an FV10i Confocal Laser Scanning Microscope (Olympus).

Cell lysis and immunoblotting. After the treatments, the cells were lysed in 20 mM Tris with 150 mM NaCl, 1% Triton X-100, 0.1% SDS, 2 mM sodium

orthovandate, 2 mM phenylmethylsulfonyl fluoride, 50 mM NaF and a protease inhibitor cocktail (Roche). The proteins were separated on a NuPAGE 10% bis-Tris midi gel (Novex) and transferred to a nitrocellulose membrane using iBlot transfer stack (Novex). The membranes were blocked for 1 h in 5% non-fat milk in PBS with 0.01% Tween-20 (PBST). After washing twice in PBST, cells were incubated with primary antibodies (Supplementary Table 2) overnight in 1% non-fat milk at 4 °C. The membranes were washed with PBST and incubated at room temperature for 2 h with secondary antibodies. The membrane was treated with chemiluminescent substrate (SuperSignal West Femto; Thermo Fisher Scientific) then imaged using a digital imaging system (Cell Biosciences).

Long-term conditioning of hMSCs using biochemical factors. For long-term conditioning, cells were incubated with the treatments as shown in Supplementary Table 3. The cells were treated with mechanical loading for 4 h each day for 7 d under sine and brachial waveform loading at 0.1 Hz and 7.5% maximum strain, or cultured under static conditions. The culture media containing the treatments were replaced on day 3 and day 5 for all treatments except for 5-Aza. Cells that were treated with 5-Aza had their culture medium replaced after 24 h with standard medium for the rest of the experiment. In some cases, culture medium was replaced with 0.5% FBS on the final day of loading to enable the collection of conditioned medium without the presence of the treatments.

Flow cytometry. For the separation of cells by markers of vascular phenotypes, the cells were detached from plate using Accutase (Sigma-Aldrich) and were labelled with fluorescent antibodies according to the BD Bioscience flow cytometry staining kit protocol (BD 562725; a list of the specific antibodies used is provided in Supplementary Table 4). For the characterization of high passage number (passage 6) and lentiviral transduced MSCs, the cells were detached from the culture plate using Accutase (Sigma-Aldrich), and were labelled with fluorescent antibodies according to the R&D Systems human mesenchymal stem cell verification flow kit protocol (R&D, FMC020; a list of the specific antibodies used is provided in Supplementary Table 4). In brief, the detached cells were centrifuged and the supernatant was removed. Fixing and permeabilizing buffer was added while the cells were vortexed and incubated for 40 min. The samples were next centrifuged and the supernatant was removed. Cells were then treated with washing buffer containing antibodies for 50 min. After antibody incubation, cells were centrifuged with washing buffer twice more, before being treated with stain buffer and measured. A BD LSR II Fortessa Flow Cytometer (BD Biosciences) was used to measure population fluorescent signals. At least 10,000 events were recorded and further gating and quantification was performed using FlowJo.

Viability flow cytometry assay. MSCs were cultured to confluency and removed from cell culture plates using 0.05% trypsin-EDTA (Thermo Fisher Scientific). A subset of the cells was treated with 90% ethanol for 1 min, then washed with PBS and centrifuged to generate a non-viable population control. Cells were labelled with fluorescent calcein-AM and ethidium homodimer-1 according to the protocol of the Live/Dead viability kit for mammalian cells (Thermo Fisher Scientific). After incubation with fluorescent dye, cells were centrifuged with washing buffer twice more, then resuspended in stain buffer. A BD LSR II Fortessa Flow Cytometer (BD Biosciences) was used to measure population fluorescence signals. At least 10,000 events were recorded and further gating and quantification was performed using FlowJo.

In vitro tube formation assay. The day before the tubule formation assay, growth-factor-reduced Matrigel (Corning) was allowed to thaw overnight at 4 °C. HUVECs (passage 5) were labelled with CellTracker Red CMTPX Dye (Thermo Fisher Scientific) and hMSCs were labelled with CellTracker Green (Thermo Fisher Scientific). These cells were then cultured in 0.5% FBS containing medium for 16 h before the tubule formation assay. On the day of the assay, glass-bottom 96-well plates were coated with 50 µl of Matrigel per well and then incubated for 30 min at 37 °C. The fluorescently labelled cells were passaged with the conditioned medium from the long-term loading onto the plates at a total seeding density of 20,000 cells per well in either hMSC alone, HUVEC alone, or a co-culture of both hMSCs and HUVECs at 1:1 ratio. These cells were then imaged at 0 h, 10 h and 22 h after seeding using Cytation 5 Cell Imaging Multi-mode Reader (Biotek) at the facilities of the Targeted Therapeutic Drug Discovery & Development Program (TTP) at UT Austin. For quantification, the number of complete loops formed was counted.

Measurement of soluble factor production. Conditioned medium was assayed for soluble factor production using an antibody array for angiogenic factors (Proteome Profiler Human Angiogenesis Array Kit; R&D Systems). Furthermore, the concentrations of some of the factors were measured using ELISA assays according to the manufacturer's instructions (R&D Systems).

Subcutaneous implantation in nu/nu mice. All of the animal studies were performed with the approval of the University of Texas at Austin Institutional Animal Care and Use Committee (IACUC) and in accordance with NIH guidelines Guide for Care and Use of Laboratory Animals for animal care. To assess the in vivo response of conditioned hMSCs, the cells were implanted subcutaneously in nu/nu mice. After 7 d of conditioning with the treatments, the cells were detached using 0.05% trypsin-EDTA and centrifuged at 200*g* for 3 min. The supernatant was removed and the cells were resuspended in Matrigel (Corning) at 2×10^6 cells per ml, in a total volume of 200 µl. These cell suspensions were then injected subcutaneously on the dorsal surface of the nu/nu mice (aged 6 weeks; Jackson Laboratories). Blood perfusion on the back of the mice was assessed using a custom speckle imaging system on days 1, 3, 5, 7 and 14 after implantation of cells[69]. Laser speckle imaging was quantified by taking the ratio of the perfusion in the region of skin over the implanted Matrigel to the perfusion of the skin over the sacral region of the mouse. After 14 d, the mice were euthanized and the tissue was collected for histological analysis.

Histochemical staining and immunohistochemistry of the skin tissues. Tissues from the subcutaneous study were cryopreserved. The subcutaneous Matrigel plug was excised using a 10 mm sterile biopsy punch. The tissues were fixed in 10% formalin in PBS for 24 h. The fixed tissues were next submerged in 30% sucrose in PBS for 4 d. Tissue samples were then frozen in isopentane cooled with liquid nitrogen. Frozen tissue samples were then sectioned (thickness, 20 µm). In brief, the frozen tissue slices were incubated in PBS for 5 min. The samples were then incubated with Fc receptor blocker (Innovex Biosciences) for 30 min and then blocked with 25% FBS in PBS for 45 min. After two washes with 1% BSA in PBS, the samples were incubated with antibodies (Supplementary Table 5) overnight followed by staining with secondary antibodies for 2 h. The antibodies used recognized both human and mouse proteins, unless otherwise specified. Samples were then mounted with Vectashield and imaged using a FV10i Confocal Laser Scanning Microscope (Olympus). For haematoxylin and eosin staining, the frozen tissues were sectioned at 10 µm before staining.

Cell encapsulation in alginate beads. The hMSCs at passage 5 were mechanically conditioned with either static, sinusoidal or brachial strain waveform at 0.1 Hz, 7.5% maximal strain for 7 d. During loading, the cells were treated with either no treatment or 1 µM E/E inhibitor biomolecule. The conditioned cells were then detached using 0.05% trypsin-EDTA, centrifuged and the supernatant removed. Approximately 1×10^6 cells were then resuspended in 200 µl alginate solution with 2% RGD peptides and 0.045% collagen. The mixture was extruded to form alginate beads with bead diameter of 1,200 µm using a coaxial airflow encapsulator (Nisco Engineering AG).

Hindlimb ischaemia model in nu/nu mice. To assess the angiogenic potential and the functional recovery induced by the MSCs, we performed a hindlimb ischaemia mice model in nu/nu mice (Jackson Laboratories). At ten weeks of age, the left femoral artery and branches were ligated to induce ischaemia. Conditioned cells were encapsulated in alginate beads as described above and then implanted onto the ischaemic leg. Blood flow through the limb was assessed using a speckle laser imaging system on days 1, 3, 5, 7, 14 and 28. The ratio between the flow though the ischaemic limb to the control limb was measured to assess recovery from ischaemia with correction for illumination intensity. After 28 d, the tissues were fixed using formalin perfusion and the muscles of the hindlimbs were collected.

RNA-seq and analysis. After treatments, RNA was isolated from the cells from four independent wells per group using the Qiagen RNeasy Mini Kit. RNA-seq was performed using an Illumina HiSeq 2500 sequencing machine. For sequencing, single reads of 50 bp were performed after poly(A) mRNA capture using the Poly(A) Tailing Kit (Ambion) and Ultra II Directional RNA Library Prep Kit (NEB) to isolate mRNA and perform dUTP directional preparation of the mRNA library. RNA-seq was performed by the Genomic Sequencing and Analysis Facility at UT Austin. Gene expression analysis was performed using R. Gene Ontology analysis was performed using the Molecular Signatures Database (En).

Histochemical staining and immunohistochemistry of the skin tissues. Muscles from the ischaemic tissues were first deparaffinized. Slides were then treated with antigen retrieval solution (Agilent) at 75 °C for 3 h. Samples were then blocked with 25% FBS in PBS for 45 min. Slides were then stained for PECAM-1 using an EnVision immunostaining kit (Agilent). In brief, the samples were blocked with dual enzyme blocker solution from DAKO. Slides were then incubated with anti-PECAM-1 antibodies (ab28364; Abcam) overnight. The next day, samples were labelled with HRP-labelled secondary antibodies for 30 min followed by extensive washes with PBS. Slides were developed with DAB chromagen for 1 min and then counterstained using Mayer's haematoxylin.

FISH analysis. Tissue slides were labelled with FISH probes according to the kit instruction from VividFISH FFPE pretreatment and VividFISH CEP probe (Genecopoeia). In brief, tissue slides were treated with pretreatment solution at 85 °C for 90 min followed up with a protease solution for 20 min. Slides were then denatured at 73 °C for 5 min, and treated with FISH probe mixed with the hybridization solution overnight at 42 °C. The next day, samples were washed and treated with DAPI mounting medium. The slides were imaged using an FV10i Confocal Laser Scanning Microscope (Olympus).

Proliferation assay. After the mechanical and chemical treatments, cells were removed from the stretch plates using 0.05% trypsin-EDTA, seeded onto optical-bottom 96-well plates at a density of 10,000 cells per well and allowed to grow for 24 h. Bromodeoxyuridine (5-bromo-2′-deoxyuridine; BrdU) labelling solution was added to culture medium. Cells were washed and stained with the detection and HRP-labelled antibodies, following the BrdU assay protocol according to the manufacturer's instructions (Cell Signaling Technology). Absorbance was read at 450 nm using a FlexStation-3 plate reader (Molecular Devices).

Permeability assay. Custom steel-bottom Transwell cell culture plates were built using polycarbonate membranes (Neuro Probe, PFD3) with 3 μm pores that are sandwiched between two plates, with silicone rubber gaskets at the interfaces to prevent leaking. The membranes were sterilized with ultraviolet light and coated with 8 μg ml^{-1} fibronectin for 4 h at 37 °C to allow cell adhesion. After coating, the fibronectin solution was removed from the top of the Transwell membranes and warm cell culture medium was added to the bottom wells of the plates. After the mechanical and chemical treatments, cells were removed from the stretch plates using 0.05% trypsin-EDTA (Thermo Fisher Scientific), seeded on top of the Transwell membranes at a density of 50,000 cells per well, and allowed to grow for 2 d. Some of the wells were left unseeded to serve as the control group. Cell culture medium was removed from the top of the Transwell plate and replaced with 200 μl of fresh culture medium containing fluorescent BSA-Texas red (diluted 1:10; Thermo Fisher Scientific) and 10 kDa dextran-Alexa Fluor 647 (diluted 1:10; Thermo Fisher Scientific). Medium (200 μl) was subsequently removed from the bottom of the Transwell plate and added to an optical-bottom 96-well plate (Thermo Fisher Scientific). Fluorescence intensity was measured using a FlexStation-3 plate reader (Molecular Devices). Culture medium devoid of fluorescent additives was included in the plate reader assay to measure background fluorescent intensity.

Transepithelial electrical resistance assay. Cells were conditioned with mechanical and chemical treatments and seeded into custom steel-bottom Transwell culture plates as described previously. Eight Transwells were left unseeded as the control group. After 2 d of growth in cell culture medium, the plates were removed from the 37 °C CO_2 cell culture incubator and allowed to cool to room temperature for 15 min. Electrodes from an epithelial ohmmeter (World Precision Instruments) were inserted into the bottom and top wells of the Transwell plate.

Bone marrow mononuclear cell isolation. Fresh ACD-A treated whole bone marrow was obtained from one human donor (StemExpress). Whole bone marrow (10 ml) was diluted with 5 ml of PBS without calcium and magnesium. The solution was distributed evenly among four 15 ml centrifuge tubes, and 5 ml of room temperature Ficoll Paque Plus (Sigma-Aldrich) was layered onto the bone marrow solution in each tube. The samples were centrifuged at 480*g* for 30 min. The resulting aqueous layer was collected, added to new centrifuge tubes and washed with PBS. This solution was centrifuged at 450*g* for 5 min and the supernatant was discarded. The cell pellet was resuspended at a density of 250,000 cells per ml and stained with flow cytometry antibodies according to the protocol described previously.

Functional identification of human MSCs. High passage (passage 6) MSCs were cultured as described above. According to the protocol from the hMSC functional identification kit (R&D Systems, SC006), cells were seeded onto glass coverslips in 24-well plates at a density of 2.1×10^4 cells per cm^2 for the adipogenic differentiation and 4.2×10^3 cells per cm^2 for the osteogenic differentiation. Cells were treated with the respectively provided differentiation medium every 3 d for a total of 21 d. After differentiation, the cells were fixed in 4% paraformaldehyde in PBS for 10 min followed by washing with PBS. Samples were next blocked and permeabilized with PBS containing 5% FBS, 1% BSA and 0.3% Triton X-100 PBS for 40 min. After washing, cells were incubated with primary antibodies (a list of the specific antibodies and concentrations is provided in Supplementary Table 1) in PBS with 1% BSA overnight at 4 °C. The samples were then washed twice in PBS with 1% BSA and incubated with secondary antibodies in PBS with 1% BSA for 2 h in a light-protected environment. Cells treated with extensive washes with PBS with 1% BSA before flipping the coverslip and mounting on glass slides in anti-fade medium (Vector Laboratories). The samples were then imaged using epifluorescence microscopy (Axio Observer; Carl Zeiss).

Oil Red O staining. After the biomechanical and chemical treatments, cells were washed with PBS and fixed with 10% formalin for 30 min. After washing with deionized water, cells were incubated with 60% isopropanol for 5 min. Oil Red O stock solution (Electron Microscopy Sciences) was reconstituted in 100% isopropanol and allowed to mix for 20 min according to the manufacturer's protocol. The working solution was diluted 3:5 with deionized water, filtered through Whatman No.1 filter paper, added to the cells and incubated for 20 min. Cells were washed until excess stain was no longer visible, and the cells were then counterstained with haematoxylin for 1 min. Cells were washed with deionized water and imaged using light microscopy.

Alizarin Red S staining. After the biomechanical and chemical treatments, cells were washed with PBS and fixed with 4% paraformaldehyde for 15 min. After washing with deionized water, cells were incubated with 40 mM Alizarin Red S (EMD Millipore) for 30 min. Cells were washed extensively with deionized water and imaged using a light microscope (Meiji).

GSEA. To define signature gene sets of ECs, pericytes and vSMCs, we downloaded multiple RNA-seq datasets (Supplementary Table 6). The obtained RNA-seq datasets were mapped to the human transcripts (GRCh38) using Salmon mapper (v.1.1.0)[70] and the count of mapped reads was normalized as transcripts per million using the R package tximport (v.1.14.2)[71]. Multiple-processed RNA-seq data belonging to each cell-type category were considered to be replicates and were compared with data obtained from MSCs using edgeR (v.3.26.8)[72] to define signature genes for each cell type. GSEA was performed using GSEA-P software (v.4.0.3)[49] with these defined gene sets ($P < 0.001$, approximately 500 genes each) and the gene expression data of the cells treated with brachial loading + E/E inhibition were compared with the control MSCs.

Endothelial and vSMC differentiation. Human MSCs (Millipore) were cultured in low-glucose DMEM medium supplemented with 15% fetal bovine serum, L-glutamine and penicillin–streptomycin. Cells were seeded onto silicone membranes coated with 50 μg ml^{-1} fibronectin. Cells were treated with 50 ng ml^{-1} VEGF-A (PeproTech) to induce endothelial differentiation, or 10 ng ml^{-1} TGF-β1 (R&D Systems) and 30 μM ascorbic acid (Sigma-Aldrich) to induce vSMC differentiation. After one week of treatment, the cells were fixed in 4% paraformaldehyde in PBS for 10 min followed by washing and permeabilization with 0.1% Triton X-100 PBS for 5 min. Samples were next blocked with PBS containing 5% FBS and 1% BSA for 40 min. After washing, cells were incubated with primary antibodies (a list of specific antibodies and concentrations is provided in Supplementary Table 1) in PBS with 1% BSA overnight at 4 °C. The samples were then washed twice in PBS with 1% BSA and incubated with secondary antibodies in PBS with 1% BSA for 2 h in a light-protected environment. Cells were washed extensively with PBS with 1% BSA before mounting in anti-fade medium (Vector Laboratories). The samples were then imaged with confocal microscopy using an FV10i Confocal Laser Scanning Microscope (Olympus).

Early osteogenic and adipogenic marker identification. After the biomechanical and chemical treatments, the cells were washed with PBS and fixed in 4% paraformaldehyde in PBS for 10 min, followed by washing and permeabilization with 0.1% Triton X-100 PBS for 10 min. Samples were next blocked with PBS containing 5% FBS and 1% BSA for 40 min. After washing, cells were incubated with primary antibodies (a list of the specific antibodies and concentrations is provided in Supplementary Table 1) in PBS with 1% BSA overnight at 4 °C. The samples were then washed twice in PBS with 1% BSA and incubated with secondary antibodies in PBS with 1% BSA for 2 h in a light-protected environment. Cells were washed extensively with PBS with 1% BSA before mounting in anti-fade medium (Vector Laboratories). The samples were then imaged by confocal microscopy using an FV10i Confocal Laser Scanning Microscope (Olympus).

Statistical analysis. All of the results are shown as mean ± s.e.m. All experiments used biological replicates that consisted of cells in non-repeated, independent cell culture wells or tissue samples from different animals, unless specified otherwise. Multiple comparisons between groups were analysed using two-way ANOVA followed by a Tukey post hoc or a Dunnett post hoc test when testing multiple comparisons versus a control group. For nonparametric data, multiple comparisons were performed using Kruskal–Wallis tests followed by post hoc testing with the Conover–Iman procedure. $P < 0.05$ was considered to be statistically significant for all of the tests.

Reporting Summary. Further information on research design is available in the Nature Research Reporting Summary linked to this article.

Data availability

The main data supporting the results in this study are available within the paper and its Supplementary Information. The source dataset for the RNA-seq analyses can be found in the NIH GEO Database (http://www.ncbi.nlm.nih.gov/bioproject/693356).

Received: 31 August 2019; Accepted: 9 December 2020;
Published online: 22 January 2021

References

1. Sarugaser, R., Hanoun, L., Keating, A., Stanford, W. L. & Davies, J. E. Human mesenchymal stem cells self-renew and differentiate according to a deterministic hierarchy. *PLoS ONE* **4**, e6498 (2009).
2. Mao, Q. et al. ILK promotes survival and self-renewal of hypoxic MSCs via the activation of lncTCF7-Wnt pathway induced by IL-6/STAT3 signaling. *Gene Ther.* **26**, 165–176 (2019).

3. Shi, Y. et al. Mesenchymal stem cells: a new strategy for immunosuppression and tissue repair. *Cell Res.* **20**, 510–518 (2010).
4. Shake, J. G. et al. Mesenchymal stem cell implantation in a swine myocardial infarct model: engraftment and functional effects. *Ann. Thorac. Surg.* **73**, 1919–1925 (2002).
5. Barbash, I. M. et al. Systemic delivery of bone marrow-derived mesenchymal stem cells to the infarcted myocardium: feasibility, cell migration, and body distribution. *Circulation* **108**, 863–868 (2003).
6. Nagaya, N. et al. Intravenous administration of mesenchymal stem cells improves cardiac function in rats with acute myocardial infarction through angiogenesis and myogenesis. *Am. J. Physiol. Heart Circ. Physiol.* **287**, H2670–H2676 (2004).
7. Muller-Ehmsen, J. et al. Effective engraftment but poor mid-term persistence of mononuclear and mesenchymal bone marrow cells in acute and chronic rat myocardial infarction. *J. Mol. Cell. Cardiol.* **41**, 876–884 (2006).
8. Cai, M. et al. PET monitoring angiogenesis of infarcted myocardium after treatment with vascular endothelial growth factor and bone marrow mesenchymal stem cells. *Amino Acids* **48**, 811–820 (2016).
9. Cai, M. et al. Bone marrow mesenchymal stem cells (BM-MSCs) improve heart function in swine myocardial infarction model through paracrine effects. *Sci. Rep.* **6**, 28250 (2016).
10. Baraniak, P. R. & McDevitt, T. C. Stem cell paracrine actions and tissue regeneration. *Regen. Med.* **5**, 121–143 (2010).
11. Cassino, T. R. et al. Mechanical loading of stem cells for improvement of transplantation outcome in a model of acute myocardial infarction: the role of loading history. *Tissue Eng. Part A* **18**, 1101–1108 (2012).
12. Watt, S. M. et al. The angiogenic properties of mesenchymal stem/stromal cells and their therapeutic potential. *Br. Med. Bull.* **108**, 25–53 (2013).
13. Yan, J., Tie, G., Xu, T. Y., Cecchini, K. & Messina, L. M. Mesenchymal stem cells as a treatment for peripheral arterial disease: current status and potential impact of type II diabetes on their therapeutic efficacy. *Stem Cell Rev.* **9**, 360–372 (2013).
14. Wagner, W. et al. Aging and replicative senescence have related effects on human stem and progenitor cells. *PLoS ONE* **4**, e5846 (2009).
15. Kretlow, J. D. et al. Donor age and cell passage affects differentiation potential of murine bone marrow-derived stem cells. *BMC Cell Biol.* **9**, 60 (2008).
16. Phinney, D. G. Functional heterogeneity of mesenchymal stem cells: implications for cell therapy. *J. Cell. Biochem.* **113**, 2806–2812 (2012).
17. Du, W. J. et al. Heterogeneity of proangiogenic features in mesenchymal stem cells derived from bone marrow, adipose tissue, umbilical cord, and placenta. *Stem Cell Res. Ther.* **7**, 163 (2016).
18. Heeschen, C. et al. Profoundly reduced neovascularization capacity of bone marrow mononuclear cells derived from patients with chronic ischemic heart disease. *Circulation* **109**, 1615–1622 (2004).
19. Hill, J. M. et al. Circulating endothelial progenitor cells, vascular function, and cardiovascular risk. *N. Engl. J. Med.* **348**, 593–600 (2003).
20. Li, T. S. et al. Impaired potency of bone marrow mononuclear cells for inducing therapeutic angiogenesis in obese diabetic rats. *Am. J. Physiol. Heart Circ. Physiol.* **290**, H1362–H1369 (2006).
21. Roobrouck, V. D., Ulloa-Montoya, F. & Verfaillie, C. M. Self-renewal and differentiation capacity of young and aged stem cells. *Exp. Cell Res.* **314**, 1937–1944 (2008).
22. Barkholt, L. et al. Risk of tumorigenicity in mesenchymal stromal cell-based therapies—bridging scientific observations and regulatory viewpoints. *Cytotherapy* **15**, 753–759 (2013).
23. Oswald, J. et al. Mesenchymal stem cells can be differentiated into endothelial cells in vitro. *Stem Cells* **22**, 377–384 (2004).
24. Li, Q. et al. VEGF treatment promotes bone marrow-derived CXCR4$^+$ mesenchymal stromal stem cell differentiation into vessel endothelial cells. *Exp. Ther. Med.* **13**, 449–454 (2017).
25. Janeczek Portalska, K. et al. Endothelial differentiation of mesenchymal stromal cells. *PLoS ONE* **7**, e46842 (2012).
26. Galas, R. J. Jr. & Liu, J. C. Vascular endothelial growth factor does not accelerate endothelial differentiation of human mesenchymal stem cells. *J. Cell. Physiol.* **229**, 90–96 (2014).
27. Henderson, K., Sligar, A. D., Le, V., Lee, J. & Baker, A. B. Biomechanical regulation of mesenchymal stem cells for cardiovascular tissue engineering. *Adv. Healthc. Mater.* **6**, 1700556 (2017).
28. Homayouni Moghadam, F. et al. Treatment with platelet lysate induces endothelial differentation of bone marrow mesenchymal stem cells under fluid shear stress. *EXCLI J.* **13**, 638–649 (2014).
29. Bai, K., Huang, Y., Jia, X., Fan, Y. & Wang, W. Endothelium oriented differentiation of bone marrow mesenchymal stem cells under chemical and mechanical stimulations. *J. Biomech.* **43**, 1176–1181 (2010).
30. Dong, J. D. et al. Response of mesenchymal stem cells to shear stress in tissue-engineered vascular grafts. *Acta Pharmacol. Sin.* **30**, 530–536 (2009).
31. Kim, D. H. et al. Shear stress and circumferential stretch by pulsatile flow direct vascular endothelial lineage commitment of mesenchymal stem cells in engineered blood vessels. *J. Mater. Sci. Mater. Med.* **27**, 60 (2016).
32. Wang, H. et al. Shear stress induces endothelial differentiation from a murine embryonic mesenchymal progenitor cell line. *Arterioscler. Thromb. Vasc. Biol.* **25**, 1817–1823 (2005).
33. Kinnaird, T. et al. Local delivery of marrow-derived stromal cells augments collateral perfusion through paracrine mechanisms. *Circulation* **109**, 1543–1549 (2004).
34. Alaminos, M. et al. Transdifferentiation potentiality of human Wharton's jelly stem cells towards vascular endothelial cells. *J. Cell. Physiol.* **223**, 640–647 (2010).
35. Tamama, K., Sen, C. K. & Wells, A. Differentiation of bone marrow mesenchymal stem cells into the smooth muscle lineage by blocking ERK/MAPK signaling pathway. *Stem Cells Dev.* **17**, 897–908 (2008).
36. Lee, J. et al. A high throughput screening system for studying the effects of applied mechanical forces on reprogramming factor expression. *Sci. Rep.* **10**, 15469 (2020).
37. Lee, J. & Baker, A. B. Computational analysis of fluid flow within a device for applying biaxial strain to cultured cells. *J. Biomech. Eng.* **137**, 051006 (2015).
38. Lee, J., Wong, M., Smith, Q. & Baker, A. B. A novel system for studying mechanical strain waveform-dependent responses in vascular smooth muscle cells. *Lab Chip* **13**, 4573–4582 (2013).
39. Serrano, I., McDonald, P. C., Lock, F., Muller, W. J. & Dedhar, S. Inactivation of the Hippo tumour suppressor pathway by integrin-linked kinase. *Nat. Commun.* **4**, 2976 (2013).
40. Crisan, M. et al. A perivascular origin for mesenchymal stem cells in multiple human organs. *Cell Stem Cell* **3**, 301–313 (2008).
41. Guimaraes-Camboa, N. et al. Pericytes of multiple organs do not behave as mesenchymal stem cells in vivo. *Cell Stem Cell* **20**, 345–359 (2017).
42. Xie, L., Zeng, X., Hu, J. & Chen, Q. Characterization of nestin, a selective marker for bone marrow derived mesenchymal stem cells. *Stem Cells Int.* **2015**, 762098 (2015).
43. Espagnolle, N. et al. CD146 expression on mesenchymal stem cells is associated with their vascular smooth muscle commitment. *J. Cell. Mol. Med* **18**, 104–114 (2014).
44. Russell, K. C. et al. Cell-surface expression of neuron-glial antigen 2 (NG2) and melanoma cell adhesion molecule (CD146) in heterogeneous cultures of marrow-derived mesenchymal stem cells. *Tissue Eng. Part A* **19**, 2253–2266 (2013).
45. Wu, C. C., Liu, F. L., Sytwu, H. K., Tsai, C. Y. & Chang, D. M. CD146$^+$ mesenchymal stem cells display greater therapeutic potential than CD146$^-$ cells for treating collagen-induced arthritis in mice. *Stem Cell Res. Ther.* **7**, 23 (2016).
46. Bussolino, F. et al. Hepatocyte growth factor is a potent angiogenic factor which stimulates endothelial cell motility and growth. *J. Cell Biol.* **119**, 629–641 (1992).
47. Kumar, A. et al. Specification and diversification of pericytes and smooth muscle cells from mesenchymoangioblasts. *Cell Rep.* **19**, 1902–1916 (2017).
48. Bhasin, M. et al. Bioinformatic identification and characterization of human endothelial cell-restricted genes. *BMC Genom.* **11**, 342 (2010).
49. Subramanian, A. et al. Gene set enrichment analysis: a knowledge-based approach for interpreting genome-wide expression profiles. *Proc. Natl Acad. Sci. USA* **102**, 15545–15550 (2005).
50. Dupont, S. et al. Role of YAP/TAZ in mechanotransduction. *Nature* **474**, 179–183 (2011).
51. Sakabe, M. et al. YAP/TAZ-CDC42 signaling regulates vascular tip cell migration. *Proc. Natl Acad. Sci. USA* **114**, 10918–10923 (2017).
52. Kim, J. et al. YAP/TAZ regulates sprouting angiogenesis and vascular barrier maturation. *J. Clin. Invest.* **127**, 3441–3461 (2017).
53. Neto, F. et al. YAP and TAZ regulate adherens junction dynamics and endothelial cell distribution during vascular development. *eLife* **7**, 31037 (2018).
54. Kato, K. et al. Pulmonary pericytes regulate lung morphogenesis. *Nat. Commun.* **9**, 2448 (2018).
55. Itoh, F. et al. Smad2/Smad3 in endothelium is indispensable for vascular stability via S1PR1 and N-cadherin expressions. *Blood* **119**, 5320–5328 (2012).
56. Hirschi, K. K., Rohovsky, S. A. & D'Amore, P. A. PDGF, TGF-β, and heterotypic cell-cell interactions mediate endothelial cell-induced recruitment of 10T1/2 cells and their differentiation to a smooth muscle fate. *J. Cell Biol.* **141**, 805–814 (1998).
57. Zonneville, J., Safina, A., Truskinovsky, A. M., Arteaga, C. L. & Bakin, A. V. TGF-β signaling promotes tumor vasculature by enhancing the pericyte-endothelium association. *BMC Cancer* **18**, 670 (2018).
58. Di Bernardini, E. et al. Endothelial lineage differentiation from induced pluripotent stem cells is regulated by microRNA-21 and transforming growth factor β2 (TGF-β2) pathways. *J. Biol. Chem.* **289**, 3383–3393 (2014).
59. Ai, W. J. et al. R-Smad signaling-mediated VEGF expression coordinately regulates endothelial cell differentiation of rat mesenchymal stem cells. *Stem Cells Dev.* **24**, 1320–1331 (2015).
60. Choi, H. J. et al. Yes-associated protein regulates endothelial cell contact-mediated expression of angiopoietin-2. *Nat. Commun.* **6**, 6943 (2015).

61. Shih, S. C. et al. Transforming growth factor beta1 induction of vascular endothelial growth factor receptor 1: mechanism of pericyte-induced vascular survival in vivo. *Proc. Natl Acad. Sci. USA* **100**, 15859–15864 (2003).
62. Tsukada, T. et al. TGFβ signaling reinforces pericyte properties of the non-endocrine mouse pituitary cell line TtT/GF. *Cell Tissue Res.* **371**, 339–350 (2018).
63. Sieczkiewicz, G. J. & Herman, I. M. TGF-β1 signaling controls retinal pericyte contractile protein expression. *Microvasc. Res.* **66**, 190–196 (2003).
64. Sato, Y. & Rifkin, D. B. Inhibition of endothelial cell movement by pericytes and smooth muscle cells: activation of a latent transforming growth factor-beta 1-like molecule by plasmin during co-culture. *J. Cell Biol.* **109**, 309–315 (1989).
65. O'Cearbhaill, E. D. et al. Response of mesenchymal stem cells to the biomechanical environment of the endothelium on a flexible tubular silicone substrate. *Biomaterials* **29**, 1610–1619 (2008).
66. Jang, J. Y. et al. Combined effects of surface morphology and mechanical straining magnitudes on the differentiation of mesenchymal stem cells without using biochemical reagents. *J. Biomed. Biotechnol.* **2011**, 860652 (2011).
67. Kim, D. H. et al. Shear stress magnitude is critical in regulating the differentiation of mesenchymal stem cells even with endothelial growth medium. *Biotechnol. Lett.* **33**, 2351–2359 (2011).
68. Wingate, K., Floren, M., Tan, Y., Tseng, P. O. & Tan, W. Synergism of matrix stiffness and vascular endothelial growth factor on mesenchymal stem cells for vascular endothelial regeneration. *Tissue Eng. Part A* **20**, 2503–2512 (2014).
69. Dunn, A. K., Bolay, H., Moskowitz, M. A. & Boas, D. A. Dynamic imaging of cerebral blood flow using laser speckle. *J. Cereb. Blood Flow Metab.* **21**, 195–201 (2001).
70. Patro, R., Duggal, G., Love, M. I., Irizarry, R. A. & Kingsford, C. Salmon provides fast and bias-aware quantification of transcript expression. *Nat. Methods* **14**, 417–419 (2017).
71. Soneson, C., Love, M. I. & Robinson, M. D. Differential analyses for RNA-seq: transcript-level estimates improve gene-level inferences. *F1000Res.* **4**, 1521 (2015).
72. Robinson, M. D., McCarthy, D. J. & Smyth, G. K. edgeR: a Bioconductor package for differential expression analysis of digital gene expression data. *Bioinformatics* **26**, 139–140 (2010).

Acknowledgements

We acknowledge funding through the American Heart Association (grant no. 17IRG33410888), the DOD CDMRP (grant nos W81XWH-16-1-0580 and W81XWH-16-1-0582) and the National Institutes of Health (grant nos 1R21EB023551-01, 1R21EB024147-01A1 and 1R01HL141761-01) to A.B.B.

Author contributions

J.L. and A.B.B. initiated the project and oversaw all aspects of the project. J.L., K.H., M.W.M., M.A.-O., B.G.I., A.V., P.M., E.Y., L.S., M.W. and A.B.B. performed experiments, processed and analysed data. B.-K.L., M.K. and J.K. performed GSEA analyses on the RNA-seq data. A.K.D. provided instrumentation and expertise in laser speckle imaging and data processing. J.L. and A.B.B. wrote and edited the manuscript. All of the authors reviewed and approved the manuscript before publication.

Competing interests

J.L. and A.B.B. have filed a patent (USPTO (US20200268801A1)) on the technology/techniques described in this paper.

Additional information

Supplementary information is available for this paper at https://doi.org/10.1038/s41551-020-00674-w.

Peer review information *Nature Biomedical Engineering* thanks Craig A. Simmons and the other, anonymous, reviewer(s) for their contribution to the peer review of this work.

Correspondence and requests for materials should be addressed to A.B.B.

Reprints and permissions information is available at www.nature.com/reprints.

Publisher's note Springer Nature remains neutral with regard to jurisdictional claims in published maps and institutional affiliations.

nature research

Corresponding author(s): Aaron Baker

Last updated by author(s): Dec 8, 2020

Reporting Summary

Nature Research wishes to improve the reproducibility of the work that we publish. This form provides structure for consistency and transparency in reporting. For further information on Nature Research policies, see our Editorial Policies and the Editorial Policy Checklist.

Statistics

For all statistical analyses, confirm that the following items are present in the figure legend, table legend, main text, or Methods section.

n/a	Confirmed	
☐	☒	The exact sample size (*n*) for each experimental group/condition, given as a discrete number and unit of measurement
☐	☒	A statement on whether measurements were taken from distinct samples or whether the same sample was measured repeatedly
☐	☒	The statistical test(s) used AND whether they are one- or two-sided *Only common tests should be described solely by name; describe more complex techniques in the Methods section.*
☒	☐	A description of all covariates tested
☐	☒	A description of any assumptions or corrections, such as tests of normality and adjustment for multiple comparisons
☐	☒	A full description of the statistical parameters including central tendency (e.g. means) or other basic estimates (e.g. regression coefficient) AND variation (e.g. standard deviation) or associated estimates of uncertainty (e.g. confidence intervals)
☐	☒	For null hypothesis testing, the test statistic (e.g. *F*, *t*, *r*) with confidence intervals, effect sizes, degrees of freedom and *P* value noted *Give P values as exact values whenever suitable.*
☒	☐	For Bayesian analysis, information on the choice of priors and Markov chain Monte Carlo settings
☒	☐	For hierarchical and complex designs, identification of the appropriate level for tests and full reporting of outcomes
☒	☐	Estimates of effect sizes (e.g. Cohen's *d*, Pearson's *r*), indicating how they were calculated

Our web collection on statistics for biologists contains articles on many of the points above.

Software and code

Policy information about availability of computer code

Data collection	No software was used.
Data analysis	Adobe Photoshop, Microsoft Excel, Metamorph, FlowJo, ImageJ, Matlab.

For manuscripts utilizing custom algorithms or software that are central to the research but not yet described in published literature, software must be made available to editors and reviewers. We strongly encourage code deposition in a community repository (e.g. GitHub). See the Nature Research guidelines for submitting code & software for further information.

Data

Policy information about availability of data

All manuscripts must include a data availability statement. This statement should provide the following information, where applicable:

- Accession codes, unique identifiers, or web links for publicly available datasets
- A list of figures that have associated raw data
- A description of any restrictions on data availability

The main data supporting the results in this study are available within the paper and its Supplementary Information. The source dataset for the RNAseq analyses can be found in the NIH GEO Database (http://www.ncbi.nlm.nih.gov/bioproject/693356).

Field-specific reporting

Please select the one below that is the best fit for your research. If you are not sure, read the appropriate sections before making your selection.

☒ Life sciences ☐ Behavioural & social sciences ☐ Ecological, evolutionary & environmental sciences

For a reference copy of the document with all sections, see nature.com/documents/nr-reporting-summary-flat.pdf

Life sciences study design

All studies must disclose on these points even when the disclosure is negative.

Sample size	For the animal studies, sizes were determined on the basis of a power calculation assuming variability similar to published studies using a similar model. For the cell-culture studies, a sample was defined as an experimental replication (not a technical replication) in all cases.
Data exclusions	No data were excluded from the analyses.
Replication	We have verified reproducibility by using independent samples, replicating key experiments multiple times, randomizing treatments for animals, and using blinded analyses and using multiple methodologies to confirm that the findings are consistent and repeatable.
Randomization	For the animal studies, the animals were randomized to the different treatments.
Blinding	The investigators were blinded to the groups during the analyses of the animal studies.

Reporting for specific materials, systems and methods

We require information from authors about some types of materials, experimental systems and methods used in many studies. Here, indicate whether each material, system or method listed is relevant to your study. If you are not sure if a list item applies to your research, read the appropriate section before selecting a response.

Materials & experimental systems

n/a	Involved in the study
☐	☒ Antibodies
☐	☒ Eukaryotic cell lines
☒	☐ Palaeontology and archaeology
☐	☒ Animals and other organisms
☒	☐ Human research participants
☒	☐ Clinical data
☒	☐ Dual use research of concern

Methods

n/a	Involved in the study
☒	☐ ChIP-seq
☐	☒ Flow cytometry
☒	☐ MRI-based neuroimaging

Antibodies

Antibodies used	These are provided in detail in the Supplemental Information (Supplementary Tables 1–5).
Validation	Information on the validation for each antibody can be found in the manufacturer's information link to the product numbers, provided in the Supplementary information.

Eukaryotic cell lines

Policy information about cell lines

Cell line source(s)	HUVECS (PromoCell), hMSCs (Millipore).
Authentication	The cell lines were confirmed by acetylated LDL uptake and marker expression (HUVEC), or by trilineage differentiation and marker expression (hMSCs).
Mycoplasma contamination	All lines were negative for mycoplasma.
Commonly misidentified lines (See ICLAC register)	No commonly misidentified cell lines were used.

Animals and other organisms

Policy information about studies involving animals; ARRIVE guidelines recommended for reporting animal research

Laboratory animals	Male and female nu/nu mice aged 8–10 weeks (from the Jackson Laboratories) were used.
Wild animals	The study did not involve wild animals.
Field-collected samples	The study did not involve samples collected from the field.
Ethics oversight	All studies were approved by the University of Texas at Austin Institutional Animal Care and Use Committee (AUP-2019-00328).

Note that full information on the approval of the study protocol must also be provided in the manuscript.

Flow Cytometry

Plots

Confirm that:

☒ The axis labels state the marker and fluorochrome used (e.g. CD4-FITC).

☒ The axis scales are clearly visible. Include numbers along axes only for bottom left plot of group (a 'group' is an analysis of identical markers).

☒ All plots are contour plots with outliers or pseudocolor plots.

☒ A numerical value for number of cells or percentage (with statistics) is provided.

Methodology

Sample preparation	Methods for processing the samples and staining are given in Methods.
Instrument	BD FACSAria III Cell Sorter
Software	Flowjo (version 10)
Cell population abundance	The abundance and purity of each group was determined according to the gating strategy given in Methods and in the Supplementary information.
Gating strategy	The gating strategy is illustrated in the Supplementary Information.

☒ Tick this box to confirm that a figure exemplifying the gating strategy is provided in the Supplementary Information.